

# Mountain permafrost in the Central Pyrenees: insights from the Devaux ice cave

Miguel Bartolomé<sup>1\*</sup>, Gérard Cazenave<sup>2</sup>, Marc Luetscher<sup>3</sup>, Christoph Spötl<sup>4</sup>, Fernando Gázquez<sup>5,6</sup>, Ánchel Belmonte<sup>7</sup>, Alexandra V. Turchyn<sup>8</sup>, Juan Ignacio López-Moreno<sup>1</sup>, Ana Moreno<sup>1</sup>

<sup>1</sup> Departamento de Procesos Geoambientales y Cambio Global, Instituto Pirenaico de Ecología-CSIC, Zaragoza, Spain.

<sup>2</sup> Société de Spéléologie et de Préhistoire des Pyrénées Occidentales (SSPPO), 5 allée du Grand Tour, 64000 PAU, France

<sup>3</sup> Swiss Institute for Speleology and Karst Studies (SISKA), La Chaux-de-Fonds, Switzerland

<sup>4</sup> Institute of Geology, University of Innsbruck, 6020 Innsbruck, Austria

<sup>5</sup> Water Resources and Environmental Geology Research Group, Department of Biology and Geology, University of Almería, Almería, Spain.

<sup>6</sup> Andalusian Centre for the Monitoring and Assessment of Global Change (CAESCG), University of Almería, Almería, Spain.

<sup>7</sup> Sobrarbe-Pirineos UNESCO Global Geopark. Boltaña. Spain.

<sup>8</sup> Godwin Laboratory for Palaeoclimate Research, Department of Earth Sciences, University of Cambridge, Cambridge, UK

\*Correspondence: Miguel Bartolomé (mbart@ipe.csic.es)

## Abstract (250 words)

Ice caves are one of the least studied parts of the cryosphere, particularly those located in inaccessible permafrost areas at high altitudes or high latitudes. We characterize the climate dynamics and the geomorphological features of Devaux cave, an outstanding ice cave in the Central Pyrenees on the French-Spanish border. Two distinct cave sectors were identified based on air temperature and

geomorphological observations. The first one comprises well-ventilated galleries with large temperature oscillations likely influenced by a cave river. The second sector corresponds to more isolated chambers, where air and rock temperatures stay below 0°C throughout the year. Seasonal layered ice and hoarfrost occupy the first sector, while transparent, massive perennial ice is present in the isolated chambers. Cryogenic calcite and gypsum are mainly present within the perennial ice. During winter, the cave river freezes at the outlet, resulting in a damming and back-flooding of the cave. We suggest that relict ice formations record past damming events with subsequent formation of congelation ice.  $\delta^{34}\text{S}$  values of gypsum indicate that the sulfate originated from the oxidation of pyrite present in the bedrock. Several features including ~~the~~ air and rock temperatures, the absence of drips, the ~~low-small~~ loss of ice in the past seven decades, and the location of ice bodies in the cave indicate that the cave permafrost is the result of a combination of undercooling by ventilation and diffusive heat transfer from the surrounding permafrost, reaching a thickness of ~200 m ~~below the surface~~.

**Keywords:** Ice cave, cave monitoring, cryogenic cave carbonates, cryogenic gypsum, ~~Devaux cave~~ Pyrenees.

## 1. Introduction

Mountain areas are ~~one of the most susceptible~~ among those environments ~~to~~ most affected by current climate change (Hock et al., 2019). In the mid-latitudes, high-altitude areas are subject to mountain permafrost, a very sensitive and unstable phenomenon that responds quickly to environmental changes (Harris et al., 2003; Biskaborn et al., 2019) due to the number of factors. ~~They influence the spatial distribution of mountain permafrost, including snow cover distribution and thickness, topography, water availability, surface temperature and rock temperature~~ Snow cover distribution and thickness, topography, water availability, and surface and rock temperature influence the spatial distribution of mountain permafrost (Gruber and Haeberli, 2009). In light of these processes, Due to this number of processes multidisciplinary studies including, among others, measurements of rock temperature ~~measurements~~ in boreholes, ~~and the~~ bottom temperatures of snow cover (BTS), ~~a variety of~~ geophysical techniques, and ~~thematic detailed maps mapping~~ (geomorphology, thermal) are needed to gain a

**Comentado [M1]:** Reviewer #2.

155-57: (R) snow cover distribution and thickness, topography, water availability, surface and rock temperature all influence the spatial distribution of mountain permafrost

**Comentado [M2]:** Reviewer #2.

157-61: (R) In light of these processes, [ ... ] are needed to gain a comprehensive understanding of mountain permafrost.

64 comprehensive understanding of mountain permafrost (e.g. [Lewkowicz and](#)  
65 [Ednie, 2004](#); [Serrano et al., 2019](#); [Biskaborn et al., 2019](#)). On the other hand, ~~the~~  
66 integrated study studies of paleo-permafrost (~~e.g. Vaks et al., 2020~~), e.g. Vaks et  
67 al., 2020) and modern permafrost, specifically mountain permafrost (e.g., [Supper](#)  
68 [et al., 2014](#); [Scandroglio et al., 2021](#)), sheds light on past, present and future  
69 developments of permafrost areas, an issue of vital importance in the context of  
70 global warming. Studies of past permafrost require sedimentary records, which  
71 are locally preserved in caves located at high altitudes and/or high latitudes.

72 Thus, temporal and spatial changes in past permafrost distribution have been  
73 identified using speleothems (stalagmites, flowstones) in high-  
74 latitude circumpolar and polar regions (e.g., Vaks et al., 2013, 2020; Moseley et  
75 al., 2021; Li et al., 2021) as well as in mid-latitude regions (e.g., Lundberg and  
76 McFarlane, 2007; Fankhauser et al., 2016; Lechleitner et al., 2020).

77 Ice caves are ~~defined as~~ cavities in rock hosting perennial ice that results from  
78 the transformation of snow and/or the freezing of infiltrating water reaching the  
79 cave ([Perşoiu and Lauritzen, 2018](#)). Cave ice can be dated and used as a  
80 valuable paleoclimate archive in non-polar areas (e.g., [Stoffel et al., 2009](#); [Spötl](#)  
81 [et al., 2013](#); [Perşoiu et al., 2017](#); [Kern et al., 2018](#); [Sancho et al., 2018a](#); [Leunda](#)  
82 [et al., 2019](#); [Munroe, 2021](#); [Racine et al., 2022](#)). ~~Furthermore, temporal and~~  
83 ~~spatial changes in past permafrost distribution have been identified using~~  
84 ~~speleothems (stalagmites, flowstones) in circumpolar and polar regions (e.g., as~~  
85 ~~well as in mid-latitude regions (e.g., Lundberg and McFarlane, 2007; Fankhauser~~  
86 ~~et al., 2016; Lechleitner et al., 2020).~~ Recently, coarse cryogenic cave carbonates  
87 (CCC<sub>coarse</sub>), that form during slow freezing of water inside caves, have been used  
88 as indicator of permafrost degradation, permafrost thickness, and subsurface ice  
89 formation ([Žák et al., 2004, 2012](#); [Richter et al., 2010a](#); [Luetscher et al., 2013](#);  
90 [Orvošová et al., 2014](#); [Spötl and Cheng, 2014](#); [Bartolomé et al., 2015](#);  
91 [Dublyansky et al., 2018](#); [Koltai et al., 2020](#); [Munroe et al., 2021](#); [Spötl et al.,](#)  
92 [2021](#)).

93 Many ice caves are located in areas where the mean annual air temperature  
94 (MAAT) outside the cave is above 0°C ([Perşoiu and Lauritzen, 2018](#)) and,  
95 therefore, are highly susceptible to future climate warming ([Kern and Perşoiu,](#)  
96 [2013](#)). These ice caves are local thermal anomalies which are controlled by the

**Comentado [M3]:** New reference added:

Li, T.-Y., Baker, J. L., Wang, T., Zhang, J., Wu, Y., Li, H.-C., Blyakharchuk, T., Yu, T.-L., Shen, C.-C., Cheng, H., Kong, X.-G., Xie, W.-L., and Edwards, R. L.: Early Holocene permafrost retreat in West Siberia amplified by reorganization of westerly wind systems, *Commun. Earth Environ.*, 2, 1–11, <https://doi.org/10.1038/s43247-021-00238-z>, 2021.

**Comentado [M4]:** Reviewer#1: lines 73-78: This sentence somehow doesn't fit to the other parts of this paragraph. Please consider omitting it or moving it to another place where it fits better.

**Con formato:** Inglés (Estados Unidos)

**Comentado [M5]:** added:

Racine, T. M. F., Reimer, P. J., and Spötl, C.: Multi-centennial mass balance of perennial ice deposits in Alpine caves mirrors the evolution of glaciers during the Late Holocene, *Sci. Rep.*, 12, 11374, <https://doi.org/10.1038/s41598-022-15516-9>, 2022.

**Con formato:** Inglés (Estados Unidos)

**Código de campo cambiado**

**Comentado [M6]:** Moved from here to lines 70-75

**Comentado [M7]:** New reference added:

Spötl, C., Koltai, G., Jarosch, A. H., and Cheng, H.: Increased autumn and winter precipitation during the Last Glacial Maximum in the European Alps, *Nat. Commun.*, 12, 1839, <https://doi.org/10.1038/s41467-021-22090-7>, 2021.

cave geometry and the associated ventilation pattern. Their ice deposits represent sporadic permafrost occurrences and do not inform about the wider thermal environment. In contrast, at high altitudes and high latitudes subsurface ice deposits are still preserved by the presence of permafrost under the current climate-conditionchange. There, mountain permafrost is limited to areas where a periglacial belt is present, with MAAT  $\leq 0^{\circ}$  C. For example, in the European Alps, discontinuous mountain permafrost is observed between-above 2600 and to 3000 m a.s.l. (Boeckli et al., 2012), while in southern Europe permafrost is generally absent (i.e. not observed even on the highest massif of the Iberian Peninsula, Gómez-Ortiz et al., 2019). In the Central Pyrenees few studies suggest the possible presence of permafrost above 2750 m a.s.l. (Serrano et al., 2019, 2020; Rico et al., 2021), and the presence of a few ice caves has only recently been documented (e.g. Sancho et al., 2018a; Serrano et al., 2018) informing about the occurrence of sporadic permafrost.-

The aim of this study is to characterize the permafrost conditions in Devaux cave, a high-altitude ice cave in the Central Pyrenees. We monitored air, water and rock temperatures and used cryogenic cave deposits to i) document the distribution of permafrost within this cave, and ii) to study the processes that resulted in perennial cave ice bodies and associated cryogenic mineral occurrences.

## 2. Study site

Devaux cave opens at ~2838 m a.s.l. in the NE cliff of Gavarnie cirque (France) of the Monte Perdido massif (MPm) in the Central Pyrenees (Fig. 1a). The cave is located between the Parc National des Pyrénées (France) and the Parque Nacional de Ordesa y Monte Perdido (Spain). Named after Joseph Devaux who discovered and explored it in 1928, the cave was later investigated with respect to its hydrogeology and microclimatology and preliminary descriptions of its deposits were reported (e.g., Devaux, 1929; 1933; Rösch and Rösch, 1935; Rösch, 1949; dDu Cailar and Dubois, 1953; Requirand, 2014).

**Comentado [M8]:** Reviewer #2

A)I90-91:

In contrast, at high altitudes and high latitudes ice deposits are still preserved under the current climate change may be in relation to the permafrost presence.

Done

**Comentado [M9]:** Reviewer #2

I98-99: (T) the presence of a few ice caves has only recently been documented

Done

**Comentado [M10]:** Reviewer #2

B) I98-99:

), informing about sporadic permafrost

Done

The area is dominated by limestones and dolostones ranging from the Upper Cretaceous to the Eocene-Paleocene. MPm is the highest limestone karst area in Europe reaching up to 3355 m a.s.l. (Monte Perdido peak) (Fig. 1b). The nearest peaks to Devaux cave are Marboré (3248 m a.s.l.) and the three Cascada peaks (3164 m, 3111 m, and 3098 m a.s.l.). The limestone thickness above the cave varies between ~200 and 250 m (Fig. 2a). In Devaux, the galleries follow the axis of a NW-SE striking syncline (Fig. 1b). A river runs along the cave (Fig. 2a, b). The cave has two known entrances: the lower one corresponds to the main outlet of the cave river (Brulle spring, North 1, ~2821 m a.s.l.), while the upper entrance is known as the “Porche” (South, ~2836 m a.s.l.) (Figs. 1c and 2b). Between these two entrances, a small gallery (Spring North 2) opens +1.2 m above Brulle spring (Fig. 1c). Brulle is one of the main springs in the Gavarnie cirque. This spring drains a catchment of ~2.6 km<sup>2</sup> (polje) located on the southern face of MPm between ~2850 and 3355 m a.s.l. (Figs. 1b and, 1d). Major water flow is observed during late spring and early summer when snowmelt ~~recharges~~ occurs in a catchment characterised by shafts, sinkholes and small closed depressions (Fig. 1d). The water of Brulle spring feeds, together with some other springs located a few hundred meters below, the Gavarnie waterfall (Fig. 1b). A tracer experiment (du Cailar et al., 1953) indicated that part of the water of the Gavarnie waterfall, and thus likely also from Brulle spring, comes from a ponor in the Lago helado (lake, Fig. 1e); located ~2.3 km to the east of Devaux cave (Figs. 1b and 2a). The Gavarnie waterfall (Fig. 1b) turned green within ~21 hours after injection of the tracer but the water at Brulle spring was not directly checked (du Cailar et al., 1953). During the colder months, the spring ~~water~~ as well as the Gavarnie waterfall freeze.

The geomorphology of the area is dominated by karst, glacial and periglacial landforms. The area was strongly glaciated during the last glacial period on both sides of the massif (e.g., Reille and Andrieu, 1995; Sancho et al., 2018b; Bartolomé et al., 2021). Today, only two glacier relicts covered by scree deposits are present in the Gavarnie cirque (Fig. 1b): 1) the Cascada dead-ice which is located several hundred meters below Devaux cave, and 2) a dead-ice accumulation in the NE wall of the cirque. Till present close to Brulle spring, on the access to Devaux and in the Cascada glacier, point to a much larger glacier

Con formato: Inglés (Estados Unidos)

161 extent in the past, maybe corresponding to the Little Ice Age or even the  
162 Neoglacial advance recognized in the nearby Tucarroya (Fig. 1b) and Troumouse  
163 cirques (Gellatly et al., 1992; González Trueba et al., 2008; García-Ruiz et al.,  
164 2014, 2020).

Con formato: Inglés (Estados Unidos)

165 The study area lies at the transition between Atlantic and Mediterranean climate,  
166 with generally cold and dry winters and warm and dry summers. In MPm, the  
167 annual ~~zero~~ 0°C isotherm is located at ~ 2900 m a.s.l. (López-Moreno et al., 2016;  
168 Serrano et al., 2019). The wet seasons are fall and spring. The annual  
169 precipitation at the Góriz meteorological station (2150 m a.s.l. and 3 km SE of the  
170 cave) averages 1650 mm. ~~However, mass balance calculations of the nearby~~  
171 ~~Monte Perdido glacier, where more than 3 m of snow (density of 450 kg/m<sup>3</sup>)~~  
172 ~~accumulates between November to April, indicates a minimum amount of 1500~~  
173 ~~mm w.e (water equivalent), therefore the total annual precipitation in~~ ~~elevate high~~  
174 ~~areas parts of the massif exceedss 2500 mm~~ ~~However, mass balance~~  
175 ~~calculations of the nearby Monte Perdido glacier suggest that annual precipitation~~  
176 ~~next to the cave may exceed 2500 mm, as the snow depth measured in early~~  
177 ~~May exceeds on average 3 m (López-Moreno et al., 2019).~~ In the MPm,  
178 discontinuous permafrost is present between ~2750 and ~2900 m a.s.l. and  
179 becomes more frequent above ~2900 m a.s.l. on the northern side (Serrano et  
180 al., 2019). Periglacial activity is characterized by rock glaciers, solifluction lobes  
181 and patterned ground (Feuillet, 2011).

Con formato: Inglés (Estados Unidos)

### 183 3. Material and methods

#### 184 3.1 Cave survey and mapping

185 A survey of Devaux cave was conducted using a compass and clinometer as well  
186 as a laser distometer (Disto-X, Heeb, 2014). In addition to cave ice, chemical and  
187 clastic deposits were mapped inside the cave. ~~These features were overlain onto~~  
188 ~~the cave survey to produce a geomorphological cave map~~ (Fig. 2b). The labelling  
189 of the cave chambers (A to K) follows the nomenclature introduced by Devaux  
190 (1929) and Röscher and Röscher (1935).

A map of potential solar radiation (RAD) of the MPm was obtained using an algorithm which considers the effects of the surrounding topography on shadowing considering the position of the sun. RAD was calculated for every month ~~of the year~~ and was then averaged to obtain an annual mean. Details of this computation can be found in [Pons and Ninyerola \(2008\)](#).

### 3.2 Cave monitoring

The cave consists of large rooms (e.g., room F, ~~or and~~ those located beyond SCAL chatière) connected by small galleries (Fig. 2b), locally with narrow passages (e.g., galleries close to SPD room or SCAL chatière, Fig. 2b). 15 stations were installed in the outmost ~350 m of the cave to monitor air (11 sensors), water (2 sensors) and rock temperature (2 sensors) (Fig. 2b). Cave air temperature variations were recorded using different devices (Hobo Pro v2 U23-001 (accuracy  $\pm 0.25^{\circ}\text{C}$ , resolution  $0.02^{\circ}\text{C}$ ), Tinytag Talk 2 (accuracy  $\pm 0.5^{\circ}\text{C}$ , resolution,  $0.04^{\circ}\text{C}$ ) and ELUSB2 (accuracy  $\pm 0.21^{\circ}\text{C}$ , resolution  $0.5^{\circ}\text{C}$ )). The cave river temperature was recorded at two points. ~~T~~ the first site (W7) was located close to the Brulle spring (Fig. 2b; Hobo TiDBit V2, accuracy  $\pm 0.21^{\circ}\text{C}$ , resolution  $0.02^{\circ}\text{C}$ ) and, the second site (W6) was located in room F (Fig. 2b; Hobo UA-001-08; accuracy  $\pm 0.53^{\circ}\text{C}$ , resolution  $0.4^{\circ}\text{C}$ ). Both sensors were installed at a water depth of 20 cm. Finally, the rock temperature was recorded at two sites (R1 and R2 in room D and K, respectively) using a Hobo U23-003 device (accuracy  $\pm 0.25^{\circ}\text{C}$ , resolution  $0.02^{\circ}\text{C}$ ). Each sensor has two external temperature probes (channels 1 and 2, Ch1-Ch2). These temperature probes were installed in two horizontal drill holes of 60 cm depth, ~1.5 to 2 m from each other.

We monitored sporadically the cave during different ~~time~~ intervals between 2011 and 2015, while a continuous monitoring was carried out between July 2017 and July 2021. ~~We calculated the m~~Maximum, minimum and mean temperatures as well as the number of frost/warm days were obtained for each sensor and site (Fig. 2b). Changes in the ice morphology were evaluated using wall marks measured at four points since 2013 in room G and using one point during 2020-2021 in room SPD (Fig. 2b) using a digital sliding caliper.

The outside temperature was measured at ~~two points in the MPm, at~~ the “Porche” entrance (~2836 m a.s.l.) and on the southern face of MPm at ~2690 m a.s.l. For

**Comentado [M11]:** Reviewer #2  
C) l183:



comparison, these temperature records were corrected assuming an adiabatic lapse rate of  $0.55^{\circ}\text{C } 100^{-1} 5.5^{\circ}\text{C km}^{-1}$  m (López-Moreno et al., 2016; Navarro-Serrano et al., 2018) to an elevation of ~2850 m a.s.l., corresponding approximately to the lower limit of the hydrological catchment area of Devaux. In both cases, the temperature was measured using Tinytag Talk 2 sensors equipped with a radiation shield. These data were compared to the temperature record from the Pic du Midi de Bigorre meteorological station (PMBS; 2011-2020) (2860 m a.s.l., ~28 km N of Devaux) obtained from Météo-France. Moreover, the homogenised MAAT dataset available since 1882 from PMBS (Bücher and Dessens, 1991; Dessens and Bücher, 1995) was-were used to identify-identify long-term climatic-temperature trends.

### 3.3 Mineralogy, water and mineral sampling X-ray diffraction, ion chromatography and sulfur isotopes

X-ray diffraction (XRD) analyses were performed on sulfate and carbonate crystals from rooms G, D and K, as well as on sulphide and oxidized crystals thereof from the host rock (Fig. S1). The analyses were performed at the Geosciences Institute in Barcelona (GEO3-BCN-CSIC) using a Bruker-AXS D5005 powder diffractometer configured in  $\theta/2\theta$ -mode (e.g. Rodríguez-Salgado et al., 2021)  $\theta$ - $2\theta$  geometry.

Samples of cave drips water, ice and river water were analysed for major ions by ion chromatography (IC) at the laboratories of the Pyrenean Institute of Ecology (Zaragoza). Carbonate alkalinity was determined by titration within 24 hours after sampling.

Sixteen samples, including sulfate crystals, dissolved sulfate and pyrite crystals were selected for sulfur isotope analyses at the Godwin Laboratory for Paleoclimate Research of the University of Cambridge (UK), following the methodology of Giesemann et al., (1994). For gypsum samples, ~5 mg of powdered gypsum were dissolved in deionized water at 45°C overnight. Then, a  $\text{BaCl}_2$  solution (50 g/L) was added to induce  $\text{BaSO}_4$  precipitation. In the case of water samples,  $\text{BaCl}_2$  was added directly to the sample. Subsequently, 6M HCl was added to remove any co-precipitated carbonate minerals and the  $\text{BaSO}_4$  precipitate was rinsed several times with deionized water. Finally,  $\text{BaSO}_4$  was

**Comentado [M12]:** Reviewer #1  
line 210: I suggest expressing the lapse rate as  $5.5^{\circ}\text{C km}^{-1}$  because the current expression is confusing. It suggests  $0.55^{\circ}\text{C}$  change by 0.01 m.

**Comentado [M13]:** Reviewer #1  
line 214: Please capitalize "Midi"

**Comentado [M14]:** Reviewer #1:  
The title of sub-section 3.3 needs revision. The current title is misleading. The section is not about sampling but about the methodology of the applied mineralogical and geochemical analyses.

**Comentado [M15]:** Reviewer #1:  
An additional related comment is that it is stated in section 4.4.2 that "XRD analyses yielded ...gypsum, calcite, ... pyrite and goethite," however no evidence is presented. I suggest adding some annotated diffractograms (at least in a supplementary document) in the revised version.

**Comentado [M16]:** Reviewer #1  
line 244: Maybe "Bragg-Brentano geometry" or " $\theta/2\theta$ -mode" would be the appropriate expression.

**Comentado [M17]:** Reference added.  
Rodríguez-Salgado, P., Oms, O., Ibáñez-Insa, J., Anadón, P., Gómez de Soler, B., Campeny, G., and Agustí, J.: Mineralogical proxies of a Pliocene maar lake recording changes in precipitation at the Camp dels Ninots (Pliocene, NE Iberia), *Sedimentary Geology*, 418, 105910, <https://doi.org/10.1016/j.sedgeo.2021.105910>, 2021.

**Con formato:** Color de fuente: Énfasis 1

**Código de campo cambiado**

**Comentado [M18]:** Reviewer #1:  
It is also quite strange that there is not any reference for the applied methods. Please consider citing the proper references in the revised manuscript.

**Comentado [M19]:** Reference added:  
Giesemann, A., Jaeger, H.-J., Norman, A. L., Krouse, H. R., and Brand, W. A.: Online Sulfur-Isotope Determination Using an Elemental Analyzer Coupled to a Mass Spectrometer, *Anal. Chem.*, 66, 2816-2819, <https://doi.org/10.1021/ac00090a005>, 1994.



dried at 45°C overnight. Sulfate~~s~~ dissolved in water were precipitated using the same method.

Isotope measurements were carried out using a Flash Elemental Analyzer (Flash-EA) at 1030 °C. The samples were folded in tin capsules. After sample combustion, the generated SO<sub>2</sub> was measured by continuous-flow gas source isotope ratio mass spectrometry (Thermo Scientific, Delta V Plus). Samples were run in duplicate and calibration was accomplished using NBS-127. The reproducibility (1σ) of δ<sup>34</sup>S was better than 0.2‰, similar to the long-term reproducibility of the standard over the run (0.2‰). δ<sup>34</sup>S isotope values are reported relative to VCDT (Vienna-Canyon Diablo Troilite).

## 4. Results

### 4.1 Devaux cave description

Devaux cave is ~2500 m long and comprises three distinct levels (Fig. 2b). The lower and the middle levels correspond to the Brulle spring (0 m), and the “Porche” entrance (~+14.5 m), respectively. The third one comprises chambers and galleries +21 m to +29 m above the Brulle spring (Fig. 2b). In the inner part of the cave, some unexplored vertical chimneys may connect to sinkholes in the catchment above the cave (Fig. 2a). The main ice deposits are located in rooms D, G, SPD and K (Fig. 2b). Except for SPD, these chambers located above the Porche entrance (between ~+1 and +7 m) can be accessed via ascending passages.

During the cold season, the cave river starts freezing at the spring and the ice then expands backward into room F (Fig. 2b). The ice totally or partially clogs the main gallery and dams the water inside the cave forming a small lake (cf. also [Rösch and Rösch, 1935](#)). This process is important for the seasonal ice extent as the flooding of the cave depends on whether the springs (North 1 and North 2) are frozen or not (e.g., [Rösch and Rösch, 1935](#)). Webcam observations (Gavarnie, Oxygène hut) suggest a possible freezing of the Brulle spring from late November to mid-May simultaneous with the freezing of the Gavarnie waterfall. Moreover, historical photos (e.g., [Devaux, 1929](#); [Rösch and Rösch, 1935](#)) and our own observations show that snow during winter and spring can

reach the Brulle entrance - a situation that also favours the blocking of the springs. As a result of such flooding events, slackwater deposits ~~are~~ present/formed in the cave entrance zone, but locally also further into the cave (e.g., in rooms I, J, K and SCAL chatière, along the main gallery; Fig. 2b), while silty sediments are found at elevated positions with respect to the river level (e.g., in rooms D and G). Sandy sediments dominate in the large rooms located beyond the SCAL chatière. Two such successions (~1 m thick) comprising hundreds of rhythmic fine-sand- ~~and~~ silt layers are present in elevated areas with respect to the current river, witnessing major events of back-flooding.

Observations made during summer show a dominant air-flow direction from the inner to the outer parts of the cave, exiting through the Brulle and Porche entrances. Conversely, the opposite is expected for the cold season (chimney effect). When the Brulle spring is partially clogged by ~~the~~ ice during early summer forcing the stream to flow below the ice, air flows from room F to C (Fig. 2b) (e.g., summer 2021). The air flow is imperceptible in rooms D, G, and close to K located away from the main cave passages.

#### 4.2 Climate setting of Devaux cave

The MAAT at the elevation of Devaux cave is ~0 °C (-0.04 °C; 2017-2021). On the other hand, a positive MAAT (1.8 °C) is recorded on the southern side of the MPm at a similar altitude (Fig. 3a). Maximum and minimum air temperatures outside the cave vary between 24.5 °C and -17.2 °C (hourly values, 2017-2021). The PMBS MAAT record (Fig. 3b) shows ~~an increase warming trend of ~+around~~ +1.5 °C since the beginning of the measurements in 1882. Before 1985, temperatures below 0°C dominated the annual cycle, while positive MAATs became more frequent in recent years. Minimum temperatures also show ~~an~~ temperature-increaseing trend of ~+2.5 °C, while the maximal annual temperatures do not show a clear trend. The north-facing Gavarnie cirque is associated with a clear RAD anomaly (Fig. 4). Values lower than 215 kWh/m<sup>2</sup> are observed at ~2000 m and between ~2800 and 2900 m a.s.l., corresponding to the cirque bottom, the area located behind La Torre peak and the surroundings of Devaux cave. At the cave site-entrance the RAD value is only 390 kWh/m<sup>2</sup>, in

**Comentado [M20]:** Reviewer #2

line 290: Please explain it a bit more what is "an increase of ~+1.5 °C". A trend value? or the difference between the mean of a certain period at the beginning and at the end of the record? or what?

**Comentado [M21]:** Reviewer #2

line 299: Please check the dimension.

stark contrast to the summit areas and surroundings where the RAD often exceeds 1500 kWh/m<sup>2</sup> (Fig. 4).

While the mean daily air temperature (MDAT) at the cave entrance (purple line in Fig. 5) and the temperature series from PMBS (pink line in Fig. 5) agree in their absolute values, the variability of MDAT at the Devaux entrance is lower than at the PMBS. This pattern could be related to local topographic conditions leading, for instance, to less RAD, or to the position of the sensor in the cliff (less night emissivity). Given this radiation contrast, warmer temperatures prevail on the southern side of the MPm (Fig. 4), favouring early snowmelt in spring and early summer, while at the same time the temperature stays below 0 °C in the cave's surroundings.

#### 4.3 Devaux cave temperature variations

The cave can be separated into distinct areas depending on their thermal regime: ventilated galleries (rooms A, B, C, F and the main gallery from SPD ~~to SCAL~~ ~~chatière~~ ~~to K~~) and ~~these poorly ventilated parts~~ off the main air flow path (rooms D, G, ~~K~~ - Figs. 2b, 5).

##### 4.3.1 Well-ventilated cave parts

Air (~~T2<sub>air</sub>, T5<sub>air</sub>, T10<sub>air</sub>, T11<sub>air</sub>~~) and water (~~W6<sub>water</sub>, W7<sub>water</sub>~~) temperature data show large seasonal oscillations. ~~at T2<sub>air</sub>, T5<sub>air</sub>, T10<sub>air</sub>, T11<sub>air</sub>, T12<sub>air</sub>, W6<sub>water</sub>, W7<sub>water</sub> and R2<sub>rock</sub> sensors.~~ All sensors except T11<sub>air</sub>, ~~T12<sub>air</sub>, and R2<sub>rock</sub>~~ show a few days with of positive temperatures during summer. Sensor T2<sub>air</sub> (2011-2012, Fig.5a), which is also the closest to the Porche entrance, shows the highest correlation (*r*) with the external temperature (0.73,  $p < 0.001$ ). ~~Sensor T5<sub>air</sub> (2017-2021, Fig. 5d) in room B also shows a high correlation and significant correlation (0.82,  $p < 0.0005$ ) with the outside temperature. During the major cave refrigeration cooling that takes place between the end of October and May and the correlation is significant and ranges between 0.68 to 0.84. During the summers and part of the falls, the correlations decreases notably (-0.23 to 0.76). -Sensor T11<sub>air</sub> (2018-2021, Fig. 5d) is located in SPD room. Despite being a well-ventilated gallery, the sensor is relatively protected from the air flow by the room morphology and shows lower correlations (-0.69,  $p < 0.001$ ) is partly protected from the air flow and shows lower a correlation (0.69,  $p < 0.001$ ) despite being located in a well-ventilated~~

Comentado [M22]: Reviewer #2

I315: I think this could be reformulated, as the authors list water, and rock T sensors together with the air T sensors.

Con formato: Color de fuente: Automático

Con formato: Color de fuente: Automático

gallery (SPD room). Also during the ~~refrigeration~~winter months, the correlations are lower (0.49-0.62,  $p < 0.001$ ) than in T5<sub>air</sub>. Sensor T5<sub>air</sub> (2017-2021, Fig. 5d) in room B also shows a high correlation with the outside temperature from November to May (0.82,  $p < 0.001$  (2017-2018); 0.66,  $p < 0.001$  (2018-2019); 0.66,  $p < 0.001$  (2019-2020); 0.86,  $p < 0.001$  (2020-2021)), while during summer and fall correlations with external temperatures are slightly weaker (0.52,  $p < 0.001$  (2017-2018); 0.37,  $p < 0.001$  (2019-2020); 0.66,  $p < 0.001$  (2020-2021)). Sensor T11<sub>air</sub> (2017-2021, Fig. 5d) is located in SPD room. Despite being a well-ventilated gallery, the sensor is relatively protected from the air flow by the room morphology and shows lower correlations (0.45,  $p < 0.001$  (2018-2019); 0.34,  $p < 0.001$  (2019-2020); 0.79,  $p < 0.001$  (2020-2021)) compared to T5<sub>air</sub>. Sensor T10 (2014-2015, Fig. 5c) does not show any significant correlation with the external temperature. Sensors T12<sub>air</sub> and R2<sub>rock</sub> are located in room K, and similar to T11<sub>air</sub>, the chamber morphology shields them from the air flow. Rock temperature sensor R2<sub>rock</sub> shows a slightly variable temperature ranging between -0.10°C and 0.28°C (mean of -0.24 and -0.23°C for channel 1 and 2, respectively). Sensor T12<sub>air</sub> shows a low correlation with the external temperature ( $r^2 = 0.35$ ,  $p < 0.001$  (2019-2021)), and the same is observed for T<sub>ext</sub>-R2<sub>rock</sub> ( $r^2 = 0.35$ ,  $p < 0.001$  (2019-2021)). Meanwhile the correlation between T12<sub>air</sub> and R2<sub>rock</sub> is high but not significant ( $r^2 = 0.93$ ,  $p > 0.005$  (2019-2021)).

The water sensors W6<sub>water</sub> and W7<sub>water</sub> (Figs. 5b, c) recorded water temperature variations during the years 2012-2013 and 2014-2015, respectively. Both sensors record a continuous temperature decline from the end of November to mid-January until the water freezes. At W7<sub>water</sub>, the temperature ranges between -0.3 and -5.8 °C between the end of fall and the beginning of winter, while between January and the beginning of June, the temperature stays close to 0°C between January and the beginning of June. At W6<sub>water</sub>, the temperature reached a minimum of -1.7 °C and shows smaller variations than at W7<sub>water</sub>. No significant correlation was found between the external air temperature and the river water temperature. Only W6<sub>water</sub> shows a weak small correlation with the external temperature when ice is absent (0.39  $p < 0.001$  and 0.40  $p < 0.001$ ).

For each monitored interval, the mean annual cave temperature at the T2<sub>air</sub>, T5<sub>air</sub> and T11<sub>air</sub> sensors is lower than the outside mean temperature for the same

**Comentado [M23]:** line 346: I suggest replacing "small" with "weak".

period (by 0.4°, 2.0°, 3.3° C lower, respectively). The W6<sub>water</sub>, W7<sub>water</sub> and T10<sub>air</sub> sensors show mean temperatures higher than the external mean temperatures (by 1.6°, 2.6°, 2.5° C higher, respectively). The periods 2011-2012 and 2017-2018 (at T2<sub>air</sub> and T5<sub>air</sub>, respectively) represent the coldest cave years of the monitoring period.

#### 4.3.2 Poorly ventilated cave parts

~~Air temperature s~~Sensors located in rooms D (T3<sub>air</sub>, T4<sub>air</sub>, T8<sub>air</sub>, ~~R1<sub>rock</sub>~~), ~~and G~~ (T9<sub>air</sub>), ~~K (T12<sub>air</sub>), and rock temperature (R1<sub>rock</sub>, R2<sub>rock</sub>)~~ show air temperatures below 0 °C during the monitoring period with small oscillations and a weak and/or insignificant correlation with the external air temperature. ~~All sensors show temperatures below 0 °C during the monitoring period with small oscillations.~~ Sensor R1<sub>rock</sub> (Fig. 5) recorded rock temperatures consistently below 0°C during the entire monitoring period. This sensor shows constant rock temperatures (-1.24 °C and -1.27 °C for channels 1 and 2, respectively), similar within error to the cave air temperature (T3<sub>air</sub>, T9<sub>air</sub>; 2019-2021). All sensors except for T3<sub>air</sub> (2011-2012, Fig. 5a) show mean air and rock temperatures lower than the mean external temperature during the same period (by 0.59 °C to 2.47°C lower). The muted temperature variations in these chambers reflect reduced heat exchange compared to the well-ventilated parts of the cave. Sensors T12<sub>air</sub> and R2<sub>rock</sub> are located in room K, and similar to T11<sub>air</sub>, the chamber morphology shields them from the air flow. Rock temperature sensor R2<sub>rock</sub> shows a slightly more variable temperature ranging between -0.19°C and -0.28°C (mean of -0.24 and -0.23°C for channel 1 and 2, respectively). Sensor T12<sub>air</sub> shows a low correlation with the external temperature ( $r^2=0.35$ ,  $p<0.001$  (2018-2021)), and the same is observed for T<sub>ext</sub> - R2<sub>rock</sub> ( $r^2=0.35$ ,  $p<0.001$  (2019-2021)). Meanwhile the correlation between T12<sub>air</sub> and R2<sub>rock</sub> is high but not significant ( $r^2=0.93$ ,  $p>0.005$  (2019-2021)).

**Comentado [M24]:** Reviewer #2

I357: I think R1 could be dropped from the list in parentheses, as it is not an air temperature sensor.

#### 4.4 Cave deposits

#### 4.4.1 Ice

Congelation ice formed by freezing of water within the cave is the most abundant type of ice, and four main ice deposits are located in chambers D, G, SPD, and K (Fig. 2b). The most relevant feature of these ice bodies is their [high](#) transparency and massive aspect, i.e. the lack of layering (Figs. 6a, b). Transparent ice is present on the ceiling, blocking chimneys, galleries and fractures. The local loss of transparency is related to the presence of cryogenic cave minerals and/or air inclusions (Figs. 6a, b, c, d).

A highly transparent ice deposit covers the southwest wall of room D and blocks the access to a gallery (Fig. 6a). The height of this deposit reaches ~6 m, and its base is located ~20 m above the Brulle spring. The thickness of this ice deposit ranges from 4.5 to 14.5 m (horizontal laser measurements across the ice in the gallery blocked by ice) and the estimated volume ranges from ~350 to ~710 m<sup>3</sup>. Three unconformities marked by cryogenic minerals were identified in this ice body.

In room G, an ice body (~25.8 to 29.6 m above the Brulle spring) is present on the ceiling (Fig. 6b) and the estimated ice volume is ~180 m<sup>3</sup>. A comparison with a historical photograph [shortly](#) before 1953 ([Casteret, 1953](#)) suggests that the ice body has not changed significantly during the last ~69 years (Figs. 7a, b). Ice-rock distances measured at four points, however, reveal small changes at three of them. The first has retreated 9.8 mm since 2014 (mean 0.9 mm a<sup>-1</sup>, n=2), the second has retreated 19.2 mm since 2014 (mean 0.6 mm a<sup>-1</sup>, n=5), and the third one has retreated 15.8 mm since 2013 (mean 2.2 mm a<sup>-1</sup>, n=7). At ~80 m from the entrance, a small descending room (SPD) (Figs. 2b, 6c) hosts a small volume of ice. Measurements between 2020 and 2021 indicate a retreat of 20 mm a<sup>-1</sup> (n=1). A last major ice deposit is present ~280 m from the entrance (room K), where transparent and massive ice (~15.5 m above the Brulle spring) ~~is currently~~ [fills a filling a](#) cupula or chimney (Figs. 2b, [6d](#)). Additional ice bodies are present behind the SCAL chatière in the upper gallery (Fig. 2b), but they have not been studied.

In contrast to these massive ice deposits, layered ice of seasonal origin is present in small chambers adjacent to the river (E and F rooms) (Fig. 6e). This ice forms

**Comentado [M25]:** Reviewer #2

I396: (T) transparent and massive ice (~15.5 m above the Brulle spring) currently fills a cupula or chimney

446 sheets of ~~around~~about 10-15 cm in thickness which are present in room F and  
447 nearby areas (Fig. 6f). This ice is related to the damming and freezing of water  
448 inside the cave when the Brulle spring freezes. Our visits from 2017 to 2021  
449 revealed that most of the damming and subsequent ice formation in room F took  
450 place during winter and spring 2017-2018 corresponding with the coldest months  
451 (both inside the cave and outside) of the monitoring period (Fig. 5d). These ice  
452 slabs are characterized by flat surfaces on both sides and obviously record  
453 incomplete freezing of the dammed water. The ice sheets largely disappeared  
454 during summer and fall, and only strongly degraded ice remained in elevated  
455 areas of room F.

456 On the other hand, ~~the~~ ice sheets associated with earlier episodes of river  
457 damming and freezing have disappeared, and only linear colour changes  
458 remained as witnesses of such events on the walls of the room E (Fig. 8d). A  
459 historical photograph exemplifies these ice levels in the access between rooms  
460 F and E (Fig. 8a). In August 1984 the ice was close to the ceiling and nearly 1 m  
461 thick (Fig. 8a; Marc Galy, pers. comm.). This contrasts with the low ice level in  
462 recent years (Fig. 8b). In total, three ice-level marks were identified in relation to  
463 back-flooding and subsequent freezing of ponded water (Figs. 8c, d). They  
464 appear at a lower elevation than the Porche entrance (c.+9.5, +9.2, +8.8, m with  
465 respect to the Brulle spring).

466 Another important feature is the presence of hoarfrost, which ~~is~~was observed in  
467 rooms A, B, C, E, F and along the gallery between SPD and ~~K-J~~ (Figs. 2b, 7g, 7h).  
468 The crystal size varies from few mm to 4 cm and appears to be upholstering some  
469 galleries and cupolas, forming aggregates that hang from the ceiling (Fig. 6h).  
470 Finally, seasonal ice formations (e.g., icicles and ice stalagmites), as well as drips  
471 are restricted to the outmost ~15 m, in the vicinity of both entrances, and in the  
472 innermost part of the cave (~ 500 m from the entrance). Seasonal ice formations  
473 are absent in cave sectors where transparent ice bodies and hoarfrost are  
474 present. Firn deposits derived from snow are restricted to the Porche entrance.

#### 476 4.4.2 Mineral deposits



They comprise mainly cryogenic cave minerals. XRD analyses of samples from rooms D, G and K yielded gypsum and calcite, while the sulfide crystals and their oxidation products present in the host rock were identified as pyrite and goethite, respectively. The presence of cryogenic gypsum in Devaux was already reported by du Cailar and Dubois (1953). In room D, gypsum was observed within the ice and on boulders (Figs. 9a, b, c). A total of three gypsum levels (lower, middle and upper, located at ~21.4, ~22.6 and ~23.9 m, respectively, with respect to the Brulle spring) were identified in the ice (Fig. 9a). Due to the progressive retreat of the ice body, some of these crystals are now present on the ice surface. Gypsum levels comprise large single crystals (0.5-1 cm in diameter), aggregates forming rafts (10 cm) up to 1 cm in thickness (Fig. 9b), as well as a fine crystalline fraction. Visual examination of the fine fraction under using a binocular stereo microscope indicates the presence of small aggregates of cryogenic cave carbonates and gypsum (CCG) (<1 mm) including globular, single and twin morphologies <1 mm in diameter (Fig. 9d).

In room G, gypsum and carbonates crystals are present in the lower part of the ice deposit (Fig. 10e) and on blocks. There, CCC are larger (>10 mm) than in room D and include globular shapes and raft-like aggregates, similar to those reported by Žák et al. (2012). Some of these CCC show gypsum overgrowths (Fig. 9f). Across the ice surface, patches of globular CCC (sub-millimetre size) have been released by ice sublimation (Figs. 7a, b). In room SPD, CCC and CCG (≤ 2 mm) are present within and on the ice (Figs. 2b, 7c). Finally, in room K, only few CCC were still present within the ice, while most of them form heaps of loose crystals covering blocks. Some of these CCCs exceed 5 mm in diameter. Crystal morphologies include rosettes, skeletons and rhombohedrons similar to those reported by Žák et al. (2012) as well as white tapered crystal aggregates. Beyond room K, regular carbonate speleothems (i.e. stalagmites, stalactites and flowstones) are present. On the contrary, gypsum crystals growing coating from walls or ceilings were not observed.

#### 4.5 Cave water chemistry and sulfate isotopic composition

**Comentado [M26]:** Reviewer #2  
I452: (T, American English spelling) millilitre

**Comentado [M27]:** Reviewer #2  
I453: (T) in room SPD, CCC and CCG

**Comentado [M28]:** Reviewer #2  
I456: for the sake of consistency, I would drop the s at the end of CCC here.

**Comentado [M29]:** Sentence added:  
On the contrary, Gypsum coating walls or ceilings was not observed.

The chemical composition of water in Devaux ~~cave (n=22) cave~~ is dominated by calcium and bicarbonate with relatively high Mg concentrations and locally also elevated sulfate concentrations (Table 1). Total dissolved solids (TDS, n=7) vary from 57 to 315 mg l<sup>-1</sup>. Devaux's dripwater has higher mean sulfate concentrations (65 mg l<sup>-1</sup>) than the cave river (11 mg l<sup>-1</sup>) and massive and seasonal ice (2.8-18 mg l<sup>-1</sup>). ~~Concerning the sulfur isotopic composition (Table 2), the~~ <sup>The</sup>  $\delta^{34}\text{S}$  value of dissolved sulfate in the dripwater is -14.4‰ (n=1), which is significantly higher than in cave river water (-28.5‰ to -27.3‰, n=2; [Table 2](#)). Gypsum crystals in room D show ~~homogeneous~~  $\delta^{34}\text{S}$  values ranging from -15.1‰ to -15.8‰ (n=7), while in room G they range from -12.3‰ to -11.9‰ (n=5). A pyrite sample from the host rock yielded a  $\delta^{34}\text{S}$  value of -12.7‰ (n=1).

## 5. Discussion

### 5.1. Processes controlling the thermal regime in Devaux cave and ~~the extent current-of~~ permafrost extent

A complex spatial distribution and a high degree of heterogeneity are among the main characteristics of mountain permafrost ([Gruber and Haeberli, 2009](#)). In Devaux cave the existence of permafrost can be related to a combination of two processes: i) cave atmospheric dynamics, and ii) conductive heat transfer through the rock.

~~Devaux cave is characterized by mean air and rock temperatures lower than the external mean annual temperature (Fig. 5). The low cave temperatures in winter lead to an inward airflow and an associated negative thermal anomaly behind the cave entrance zone. On the contrary, during summer, the cold and dense air flows out of the cave due to the temperature difference between outside and inside air. Also, the heat supplied to the cave by the river can also modify influences the cave air temperature by exporting thermal energy. Thus, this process drags cold outside air into the cave during winter and on the contrary during summer. Devaux cave is characterized by mean air and rock temperatures lower than the external mean annual temperature (Fig. 5). The low cave temperatures in winter lead to an inward airflow and an associated negative thermal anomaly behind the cave entrance zone. Similar seasonal ventilation~~

**Comentado [M30]:** Reviewer #2

E) I315 - figure 5d, the air temperature variations at T11 and T5 (and T2) could be discussed in additional detail (at line 481 for instance).

patterns have been observed in ice caves elsewhere (e.g., Luetscher et al., 2008; Colucci and Guglielmin, 2019; Perşoiu et al., 2021).

On the other hand, positive temperatures are observed both in the cave river and in the air at the cave entrance (Fig. 5), reflecting heat advected by water (river) and the influence of the external temperature (cf. Luetscher et al., 2008; Badino, 2010). The lack of correlation between the external and internal temperatures and the small temperature variability in rooms D, G, and K reflect their thermal isolation from well-ventilated cave parts. There, the apparent thermal equilibrium between the rock and the cave atmosphere ( $T_{\text{rock}}=T_{\text{air}}$ ) supports the notion that heat exchange is dominated by conduction through the bedrock.

The MAAT at the altitude of the cave is  $-0.04\text{ }^{\circ}\text{C}$  (2017-2021) suggesting that the  $0\text{ }^{\circ}\text{C}$  isotherm is located close to the cave. Using an array of techniques (geomatic surveys, temperature monitoring, temperature at the base of the snowpack (BTS) and geomorphological and thermal mapping), Serrano et al. (2019) found observed mean annual ground temperatures between  $-1$  and  $-2\text{ }^{\circ}\text{C}$  on the northern slope of the MPm suggesting that discontinuous permafrost is present between 2750-2900 m a.s.l., with more continuous permafrost starting at 2900 m a.s.l. The orientation of the Gavarnie cirque, as well as the high slope angle, and shadow from the surrounding peaks favour the preservation of permafrost at lower elevations (e.g., Gubler et al., 2011).

Given the high thermal inertia of the rock, the permafrost temperature at depth is still under the influence of past climate conditions (e.g., Haeberli et al., 1984; Noetzi and Gruber, 2009) and, therefore, part of the current permafrost in the area could be inherited from previous colder times (e.g., Colucci and Guglielmin, 2019). In particular, the low mean annual temperatures recorded at PMBS at in the late 19<sup>th</sup> century the beginning of the Industrial Era were favourable conditions for permafrost development in the recent past. We surmise that the current permafrost could be inherited from colder periods of the Little Ice Age.

In well-ventilated ice caves hoarfrost is the most dynamic ice formation on seasonal time scales. The presence of perennial hoarfrost is, however, indicative of a continuously frozen bedrock and thus representative of caves within the

**Comentado [M31]:** Reviewer #2

I501: (T) with more continuous permafrost starting at 2900 m asl

**Comentado [M32]:** Reviewer #2

D) I506-513

**Comentado [M33]:** Reviewer #1.

line 511: I suggest replacing the term "beginning of the Industrial Era" with "late 19<sup>th</sup> century". As far as I know the Industrial Era begun much earlier than the PMBS record.

permafrost zone (e.g. Luetscher and Jeannin, 2018; Yonge et al., 2018). In Devaux cave, perennial hoarfrost is observed in rooms where the bedrock is surrounded by small ice bodies (e.g., gallery close to SPD room, Fig. 6g). Devaux (1929) indicated the presence of ice crystals on the ceiling at the entrance of room D. In the same way, du Cailar and Dubois (1953) showed a schematic cross-section of room D, where ice crystals are present at the beginning of the room. These historical reports suggest these areas were probably more ventilated in the past, which favoured the hoarfrost formation. -On the other hand, seasonal hoarfrost is present in ventilated galleries (A, B, C, F and between SPD and J). Seasonal hoarfrost in room B and C, and in the area between H to J, disappears at the end of summer, probably because of the heat delivered by the cave river, as recorded by the T5 sensor (Fig. 5).

The presence of permafrost in Devaux's catchment is supported by the absence of drips and/or seepage in the investigated cave passages (e.g., Luetscher and Jeannin, 2018; Vaks et al., 2020). Active drips and seasonal ice formations are limited to the first ~15 m of the cave as well as to the inner part (beyond room K). Mountain permafrost thus penetrates ~350 m longitudinally from the East-eastern cliff of the Gavarnie cirque to the southern side of the massif, following a west-east direction. On the other hand, given the elevation of the cave and the topographic-topography relief above the cave, the current maximum permafrost thickness (without taking into account the active layer) on the southern side of the MPm is ~200 m (without taking into account the active layer).

## 5.2. The origin of ice in Devaux cave

The transparent and massive character of Devaux's cave ice, as well as the presence of CCC, which formation requires low congelation rates (Žák et al., (2004)), suggests that this ice formed by slow freezing of water dammed by ice at the spring. This model is consistent with the climate in-of the Gavarnie cirque, cave geomorphological observations, cave air and water temperatures as well as historical reports. The cave water level can rise by several meters as indicated by slackwater deposits upstream of the Brulle spring.

### Comentado [M34]: Reviewer 2:

G) I518 - the only place where perennial hoarfrost is indicated on figure 2B is a small recess appears to be surrounded by ventilated galleries containing seasonal hoarfrost, and as mentioned adjacent to a small ice body of room SPD. This certainly speaks to the frozen nature of the bedrock in this part of the cave, and demonstrates the clear effect of the negative thermal anomaly brought about by the ventilation pattern in the surrounding galleries. But if this is the case, could the authors comment on why there is no perennial hoarfrost in the galleries leading to room D, where such hoarfrost could also have developed?

### Comentado [M35]:

Reviewer #2

I535-536: massive ice is formed by slow freezing - there should perhaps be a reference here.

The distribution and characteristics of ice bodies in Devaux cave indicate that the hydraulic head rose by at least ~ 15 - 29 m, which is the elevation of the ice bodies in rooms G, F and K. This situation requires that all springs (including Porche) are blocked for a sufficiently long time to allow for complete freezing of these cave lakes. The lack of important unconformities in this massive ice (e.g., detrital layers), which are usually related to seasonal ablation (e.g., [Luetscher et al., 2007](#); [Stoffel et al., 2009](#); [Hercman et al., 2010](#); [Spötl et al., 2013](#)), suggests that the ice deposit in room G it is the result of a single flood event. On the contrary, the small unconformities recognized in the ice body in room D suggest that several cycles of damming and subsequent ice formation cannot be discarded in the formation of this ice deposit.

~~Our~~ These observations indicate that under the current climate (both in the cave and outside) only part of the water dammed in rooms F and E freezes during winter and spring. This strongly suggests that the ice bodies in Devaux cave must have been associated with colder and/or longer events of ponding and freezing than today, when the cave was effectively sealed from the outside for prolonged times. We hypothesize that the advance of a glacier on the steep slopes of Devaux's surroundings could have contributed to the blockage of the spring, leading to backflooding and the formation of large ice bodies in the cave. In the study area, such periods of glacier growth occurred during the Little Ice Age and/or the Neoglacial ([González Trueba et al., 2008](#); [García-Ruiz et al., 2014, 2020](#)).

The freezing of a flooded cave passage cannot be explained by the advection of cold air alone. It is thus surmised that heat transfer through the host rock is a more plausible mechanism for the complete freezing of the ponded water. The cave ice bodies; just as well as the presence of cryogenic minerals; therefore represents a record of a long cold period or of several such shorter episodes. Although the cryogenic minerals and in particular CCC<sub>coarse</sub> are typically associated with permafrost thawing during warm spells ([Žák et al., 2004](#); [Richter et al., 2010](#); [Žák et al., 2012](#); [Luetscher et al., 2013](#)), permafrost conditions prevailed during ice formation in Devaux cave. Thus, the water that feeds

**Comentado [M36]:** Reviewer #1

lines 546-552: Discordancy without visible detrital layer could also indicate unconformity. A nice example can be found in Fig5 of Hercman et al., 2010 ([http://www.geochronometria.pl/pdf/geo\\_36/Geo36\\_05.pdf](http://www.geochronometria.pl/pdf/geo_36/Geo36_05.pdf)). This type of discordancy/unconformity could be also considered in this part of the discussion.

**Comentado [M37]:** Reference added:

Hercman, H., Gąsiorowski, M., Gradziński, M., and Kicińska, D.: The First Dating of Cave Ice from the Tatra Mountains, Poland and its Implication to Palaeoclimate Reconstructions, *Geochronometria*, 36, 31–38, <https://doi.org/10.2478/v10003-010-0016-2>, 2010.

**Comentado [M38]:** Reviewer #1:

line 554: Maybe “These” instead of “Our”.

**Comentado [M39]:** Reviewer #2

l568: (T) The cave ice bodies [...] therefore represent

636 Devaux's springs infiltrated during late spring and summer from ponors at Lago  
637 helado and/or surrounding ~~poljes, (which may have acted as local taliks).~~  
638 However, the heat supplied by this water may have probably not been enough to  
639 thaw the frozen host rock. It is thus very likely that the hostrock temperature was  
640 ~~much~~ lower and/or the outlets remained closed ~~for~~ longer ~~periods~~ than today to  
641 allow for the complete ~~slow~~ freezing of the ponded water.

**Comentado [M40]:** Reviewer #2:

lines 574-575: I suggest omitting the bracketed comment.

642

### 643 5.2.1 Ice volume changes

644 The colour changes in the walls close to the river (room E), the historical  
645 photograph as well as speleological reports point to large changes (several  
646 meters) ~~of in~~ the height of the seasonal ice in the flood-prone sector of the cave  
647 (Figs. 8a, b). This ice is influenced by the heat exchanged between the water and  
648 the cave.

649 In contrast, changes in the ice volume are almost negligible in rooms D and G  
650 where the temperature is more constant and below 0°C (Figs. 7a, b). The ice  
651 body in room G ~~has been retreats-retreating only~~ by ~~only~~ ~0.6 to ~2.2 mm a<sup>-1</sup>. A  
652 similar value (3 mm a<sup>-1</sup>) was observed in Coulthard cave (Alberta, British  
653 Columbia, Marshall and Brown, 1974), a cave located ~~with~~in permafrost (Yonge  
654 et al., 2018). Changes in the ice body in this cave were related to slow sublimation  
655 due to convective air flow inside the cave (Marshall and Brown, 1974). On the  
656 other hand, the ice in SPD room shows higher ice retreat rates (~ 20 mm a<sup>-1</sup>).  
657 Similar sublimation rates have been reported in ~~others~~ ice caves in the Pamir  
658 Mountains and the northern part of the Russian Platform (Mavlyudov, 2008; Žák  
659 et al., 2018). Overall, Devaux's cave ice deposits ~~show~~ a remarkable stability  
660 which contrasts ~~to with~~ the rapid changes observed in ice caves outside  
661 permafrost areas (Kern and Perşoiu, 2013; Perşoiu et al., 2021; Wind et al.,  
662 2022), including other ice caves in the Pyrenees and Picos de Europa (Belmonte-  
663 Ribas et al., 2014; Gomez-Lende et al., 2014, 2016).

**Comentado [M41]:** Reviewer #2

I596: (T) which contrasts with

**Con formato:** Inglés (Estados Unidos)

664

### 665 5.3. Cryogenic cave minerals

In Devaux cave, CCC and CCG are still present within the ice (Figs. 6, a, b, c, d). Worldwide, only very few *in situ* observations of coarse-grained cryogenic cave minerals are known (e.g., Bartolomé et al., 2015; Colucci et al., 2017). du Cailar and Dubois (1953) reported the presence of gypsum crystals at ~50 cm depth within the ice in Devaux cave. The first evidence of *in situ* CCC<sub>coarse</sub> in cave ice was reported from Sarrius 6, an ice cave at 2780 m a.s.l. on the southern slope of the MPm (Bartolomé et al., 2015). Colucci et al. (2017) documented the presence of CCC<sub>coarse</sub> in a small ice cave in the Italian Alps. Recently, Munroe et al. (2021) found CCC<sub>coarse</sub> in ice of Winter Wonderland cave (Utah, USA). Because of the abundance of cryogenic cave minerals, the size of individual crystals and aggregates thereof, and their varied-different mineralogy, Devaux cave provides an additional opportunity for studying the origin of such cryogenic cave minerals.

The CCGs in Devaux cave represents, to our knowledge, the first occurrence of its kind in a carbonate karst terrain. So far, CCGs have only been reported from gypsum karst areas in Russia and Ukraine (Korshunov and Shavrina, 1998; Žák et al., 2018 and references therein). In those areascaves, tiny gypsum crystals (gypsum powder) form during rapid freezing of water. When ice sublimates in winter, this-these gypsum-particles powder-isare released and accumulates as powdery deposits on the ice surface. Eventually, they partly powder dissolves on the ice surface during spring and summer due to the increase in cave air humidity, and later recrystallizes forming a wide variety of delicate-crystal morphologies. CCGs from Devaux cave shows features that do not correspond to those previously published from gypsum karst caves. In particular, the Devaux cave CCGs i) appears together with CCC<sub>coarse</sub> crystals (≥5 mm in some cases, in rooms D and G), ii) the (raft-like) gypsum crystals are large (Fig. 9b) and, in some cases, are still found within the ice (Fig. 9a) and surrounded by milky ice rich in air inclusions (Fig. 9a, e), and iii) boulders are locally overgrown by gypsum (Fig. 9c).

Coarse-grained cryogenic cave minerals form in a semi-closed system, when the water freezes very slowly freezes inside the caves at low freezing rates (Žák et al., 2004). Once supersaturation is reached, CCM start to crystallize. The

**Comentado [M42]:** Reviewer #2  
l615: for the sake of consistency, drop s at the end of CCG here.



formation of gypsum crystals requires the presence of [elevated concentrations of](#) dissolved sulfate which may relate to i) sedimentary gypsum deposits intercalated within carbonates (e.g., [Sancho et al., 2004](#)), ii) the presence of hydrothermal water [containing](#)  $H_2S$  ~~in relation with~~ [related to](#) hydrocarbons (e.g., [Hill, 1987](#)), or iii) the oxidation of sulfides (e.g., pyrite) disseminated in ~~limestones-carbonate~~ [rocks](#) (e.g., [Bottrell, 1991](#)). In the case of Devaux cave marine evaporite rocks (e.g., of the Upper Triassic Keuper facies) and hydrocarbons are absent in the catchment of the cave. The most plausible explanation for the presence of dissolved sulfate in Devaux's water is the oxidation of pyrite present in the limestone ([du Cailar and Dubois, 1953](#); [Requirand, 2014](#)).

**Comentado [M43]:** I636: (T) related to hydrocarbons

~~Water in Devaux cave contains moderate concentrations of sulfate.~~  $\delta^{34}S$  values of gypsum (-11.9 to -15.8 ‰), pyrite (-12.7 ‰), and dissolved sulfate (-14.4 ‰ in dripwater and -28.5 to -27.3 ‰ in Brulle spring water) are within the range of biogenic pyrite and differ notably from values of marine evaporites (10-35 ‰) ([Seal, 2006](#)). Thus, the  $\delta^{34}S$  values together with the geological setting of the cave support the hypothesis that disseminated pyrite in the host limestone is the main source of dissolved sulfate and subsequently of CCG. Only the dissolved sulfate  $\delta^{34}S$  values of Brulle spring are considerably more negative (-28.5‰ and -27.3‰). This may be a consequence of microbially mediated redox processes in the karst that discriminate against  $^{34}S$  ([Zerkle et al., 2016](#); [Temovski et al., 2018](#)). Further studies on the microbiology of the cave may shed light on these mechanisms and how the local sulfur cycle may have changed in the [recent](#) past.

In gypsum caves, dissolved sulfate dominates over the bicarbonate, and the typical crystallization sequence during freezing of water with high TDS is gypsum → carbonate (commonly calcite) → celestine ([Žák et al., 2018](#)). In Devaux cave, however, bicarbonate dominates over sulfate, and our observations show that gypsum crystals partly nucleated on  $CCC_{coarse}$ . Accordingly, the crystallization sequence at Devaux cave is calcite → gypsum, taking place in a semi-closed system at low freezing rates.

The second aspect that makes the CCG in Devaux ~~cave~~ unique is the size and ~~well-developed euhedral~~ [crystal](#) shapes of the crystals (Fig. 9 b), which differ

**Comentado [M44]:** I666-667: (T) is the size and well-developed shape of the crystals

notably from the much smaller sizes of gypsum crystals (20-200  $\mu\text{m}$ ) and gypsum powders (1-30  $\mu\text{m}$ ) found in gypsum caves in Russia and Ukraine (Žák et al., 2018 and references therein). Another characteristic of CCC and CCG occurrences in Devaux cave is the presence of milky ice surrounding them (Fig. 9a, e) which seems to be related to the freezing process during the formation cryogenic minerals in a subaqueous environment. Similar to that, CCC were found within the ice and surrounded by bubbles in Sarrius 6 ice cave (Bartolomé et al., 2015). However, the scarce presence of CCC within the ice today, together with the very few sites where this topic is investigated, leads to a lack of studies about gas inclusions and CO<sub>2</sub> degassing during CCC formation.

**Comentado [M45]:** Reviewer 2

H) Could the authors elaborate on why CCC or CCG related ice, rich in air inclusions could be related to the formation in a subaqueous environment?

Finally, the presence of gypsum aggregates overgrowing ~~some~~ blocks (Fig. 9c) supports the hypothesis of subaqueous gypsum formation. On the other hand, the absence of gypsum was never observed growing from on the ceiling or on the walls, thus allowing it to discard its formation from seepage water followed by precipitation due to evaporation in the cave (e.g., Gázquez et al., 2017, 2020). In essence, all observations indicate that gypsum precipitated in a semi-closed subaqueous environment and has been preserved from later dissolution by the exceptionally dry environment of this ice cave. Gypsum precipitating from freezing waters has been also documented in the Arctic and the Antarctica (Losiak et al., 2016; Wollenburg et al., 2018) and has been proposed as a mechanisms for gypsum formation on Mars (Losiak et al., 2016).

**Comentado [M46]:** Reviewer #1

lines 676-679: I think that this info could be moved forward in the section.

## 6. Conclusions

The investigation of Devaux ice cave, based on cave monitoring, geomorphology, and geochemical analyses, provides exceptional insights into the origin of modern and past mountain permafrost and associated processes and deposits.

- Devaux cave consists of two parts characterised by different thermal regimes:

- 1) the near-entrance parts and the main gallery showing large temperature fluctuations and cave air temperatures seasonally exceeding 0°C. These passages are influenced by ~~an~~ advective air flow and ~~the~~ heat released by the cave river.
- 2) The inner sector and isolated chambers are characterized by muted thermal oscillations and temperatures constantly below 0°C. There, the

cave air temperature is mainly controlled by heat conduction through the bedrock.

- Devaux cave is impacted by backflooding in late winter/early spring when the main outlets freeze, damming the water inside the cave forming a lake. The blocking of the outlets requires temperatures below 0°C in the Gavarnie cirque, while on the southern side of the Monte Perdido massif, temperatures above 0°C allow water infiltration.

- The absence of dripwater in most parts of the cave together with the presence of perennial/seasonal hoarfrost, and the location of massive ice bodies on the ceiling and/or filling cupulas and galleries are indicative of frozen bedrock surrounding the cave. Permafrost at Devaux cave is attributed to a combination of rock undercooling by cave air ventilation and the local climate setting giving rise to the development and/or preservation of permafrost inherited from past colder periods. Currently, permafrost seems to be present above the cave reaching a maximum thickness of ~200 m and a lateral extension of ~350 m towards the southern face of the Monte Perdido massif.

- We report the first deposits of cryogenic gypsum in a limestone-hosted ice cave. Most of the cryogenic minerals are still within the ice and surrounded by milky ~~ice~~ ~~ice~~-rich in air ~~inclusions~~. Gypsum precipitation occurred subaqueously as a result of slow freezing, following CCC formation.  $\delta^{34}\text{S}$  values show that the sulfate originated from the oxidation of pyrite present in the limestone.

- Current climate conditions seem to be still favourable for the preservation of ice within this cave. This situation contrasts to the large ~~ice mass loss~~ in other ice caves elsewhere. The ice deposits in Devaux ~~cave~~ allow unique insights into processes leading to the formation of cryogenic carbonates and sulfates, and represents ~~an ideal~~ ~~a~~ unique site to better understand the mountain permafrost evolution in the Monte Perdido massif and the Pyrenees in general.

## Competing interests

No competing of interest

**Comentado [M47]:** Reviewer #2:  
l718: (T) rich in air inclusions

**Comentado [M48]:** Reviewer #1  
line 723: Please consider adding "ice mass" between the word large and loss to clarify the meaning of the sentence.

**Comentado [M49]:** Reviewer #2  
l724: (T) in Devaux cave

#### Authors contribution

MB conceived the project, planned fieldwork and the sampling strategy. AM obtained funding for this work. MB and GC installed and maintained the sensors and performed the fieldwork. GC contributed with cave monitoring data from 2011 to 2015. MB analysed monitoring, geomorphological, and geochemical data. FG performed  $\delta^{34}\text{S}$  analyses using the facilities provided by AVT. JILM created the radiation map. MB designed the figures and wrote a first draft of the manuscript. ML and CS significantly contributed to the discussion of the data. ML and AM reviewed all versions of the manuscript. All authors reviewed the manuscript and contributed to the results, discussion, and final interpretation. All authors approved its submission.

#### Acknowledgements

We thank the directorates of the Parc National des Pyrénées (France) and the Ordesa y Monte Perdido National Park (Spain) for their permission to investigate Devaux cave. We want to especially thank Marc Galy for his cave survey which improves noticeably previously published surveys and for the historical photo of 1984. Also, we thank Météo France for providing climate data from the Pic du midi de Bigorre station. We thank Maria Leunda for a critical review and suggestions to the first draft of the manuscript. We also thank Jerome Labat (SSPPO), Claude Novoa, Alvaro Palacios, Maria Leunda, José Leunda, David Serrano, the Góriz hut staff ([www.goriz.es](http://www.goriz.es)), and the Palazio family ([www.hotelpalazio.com](http://www.hotelpalazio.com)) for their invaluable help during fieldwork. We thank Paul Cluzon for the photo of Fig. 1d, and Claude Requirand for his report about Devaux cave. The authors would like to acknowledge the use of the Servicio General de Apoyo a la Investigación-SAI, University of Zaragoza, and Alberto Barcos (IPE-CSIC) for the chemical water analyses. This study contributes to the work carried out by the DGA research group Procesos Geoambientales y Cambio Global (ref.: E02-20R) and the MERS research group 2017 SGR 1588.

#### Financial support

This research has been supported by the following projects which were funded by the National Parks Autonomous Agency (OAPN) (OCHESTRA-ref 2552/2020), the Spanish Agencia Estatal de Investigación (AEI-Spain)

(PICACHU-ref PID2019-106050RB-I00), (SPYRIT- ref CGL2016-77479-R), the PaleolCE EXPLORA project (ref. CGL2015-72167-EXP) and the Comité régional de spéléologie de Nouvelle Aquitaine. Miguel Bartolomé was supported by a postdoctoral fellowship of the Juan de la Cierva-Formación program provided by the Spanish Ministry of Science (ref.: FJCI-2017-31725) and OCHESTRA-ref 2552/2020. Fernando Gázquez was financially supported by a Ramón y Cajal Fellowship (RYC2020-029811-I) of the Spanish Government (Ministerio de Economía y Competividad).

## References

- Badino, G., 2010. UNDERGROUND METEOROLOGY-“What’s the weather underground?” *Acta Carsologica* 39. <https://doi.org/10.3986/ac.v39i3.74>
- Bartolomé, M., Sancho, C., Benito, G., Medialdea, A., Calle, M., Moreno, A., Leunda, M., Luetscher, M., Muñoz, A., Bastida, J., Cheng, H., Edwards, R.L., 2021. Effects of glaciation on karst hydrology and sedimentology during the Last Glacial Cycle: The case of Granito cave, Central Pyrenees (Spain). *CATENA* 206, 105252. <https://doi.org/10.1016/j.catena.2021.105252>
- Bartolomé, M., Sancho, C., Osácar, M.C., Moreno, A., Leunda, M., Spötl, C., Luetscher, M., López-Martínez, J., Belmonte, A., 2015. Characteristics of cryogenic carbonates in a Pyrenean ice cave (northern Spain). *Geogaceta* 58 107–110.
- Belmonte-Ribas, Á., Sancho, C., Moreno, A., Lopez-Martinez, J., Bartolome, M., 2014. Present-day environmental dynamics in ice cave a294, central pyrenees, spain. *Geogr. Fis. E Din. Quat.* 37, 131–140. <https://doi.org/10.4461/GFDQ.2014.37.12>
- Biskaborn, B.K., Smith, S.L., Noetzi, J., Matthes, H., Vieira, G., Streletskiy, D.A., Schoeneich, P., Romanovsky, V.E., Lewkowicz, A.G., Abramov, A., Allard, M., Boike, J., Cable, W.L., Christiansen, H.H., Delaloye, R., Diekmann, B., Drozdov, D., Etzelmüller, B., Grosse, G., Guglielmin, M., Ingeman-Nielsen, T., Isaksen, K., Ishikawa, M., Johansson, M., Johannsson, H., Joo, A., Kaverin, D., Kholodov, A., Konstantinov, P., Kröger, T., Lambiel, C., Lanckman, J.-P., Luo, D., Malkova, G., Meiklejohn, I., Moskalenko, N., Oliva, M., Phillips, M., Ramos, M., Sannel, A.B.K., Sergeev, D., Seybold, C., Skryabin, P., Vasiliev, A., Wu, Q., Yoshikawa, K., Zheleznyak, M., Lantuit, H., 2019. Permafrost is warming at a global scale. *Nat. Commun.* 10, 264. <https://doi.org/10.1038/s41467-018-08240-4>
- Boeckli, L., Brenning, A., Gruber, S., Noetzi, J., 2012. A statistical approach to modelling permafrost distribution in the European Alps or similar mountain ranges. *The Cryosphere* 6, 125–140. <https://doi.org/10.5194/tc-6-125-2012>
- Bottrell, S.H., 1991. Sulphur isotope evidence for the origin of cave evaporites in Ogof y Daren Cilau, south Wales. *Mineral. Mag.* 55, 209–210. <https://doi.org/10.1180/minmag.1991.055.379.09>
- Bücher, A., Dessens, J., 1991. Secular Trend of Surface Temperature at an Elevated Observatory in the Pyrenees. *J. Clim.* 4, 859–868. [https://doi.org/10.1175/1520-0442\(1991\)004<0859:STOSTA>2.0.CO;2](https://doi.org/10.1175/1520-0442(1991)004<0859:STOSTA>2.0.CO;2)
- Casteret, N., 1953. Dans les glaces souterraines. Les plus élevées de Monde. Librairie Académique Perrin, Paris, p. 93.

- Colucci, R., Luetscher, M., Fortee, E., Guglielmin, M., Lenaz, D., Princivalle, F., Vita, F., 2017. First alpine evidence of in situ coarse cryogenic cave carbonates (CCCcoarse). *Geogr. Fis. E Din. Quat.* 53–59. <https://doi.org/10.4461/GFDQ.2017.40.5>
- Colucci, R.R., Guglielmin, M., 2019. Climate change and rapid ice melt: Suggestions from abrupt permafrost degradation and ice melting in an alpine ice cave. *Prog. Phys. Geogr. Earth Environ.* 0309133319846056. <https://doi.org/10.1177/0309133319846056>
- Dessens, J., Bücher, A., 1995. Changes in minimum and maximum temperatures at the Pic du Midi in relation with humidity and cloudiness, 1882–1984. *Atmospheric Res., Minimax Workshop* 37, 147–162. [https://doi.org/10.1016/0169-8095\(94\)00075-0](https://doi.org/10.1016/0169-8095(94)00075-0)
- Devaux, J., 1929. Nouvelle grotte Marboréenne. *La Natura* 102–107.
- Devaux, J., 1933. La grotte des sœurs de la cascade. Études glaciologiques, 1920-1930. Tome VII, pp. 233-238. Plan & coupe. Paris. Imprimerie Nationale. Ministère de l'Agriculture. Direction des eaux et du génie rural.
- du Cailar, J., Couderc, J., Dubois, P., 1953. La source du Gave de Pau. *Annales de Spéléologie* 181–203.
- du Cailar, J., Dubois, P., 1953. Sur quelques modalités de formation et d'évolution des dépôts cristallins dans les cavités de haute altitude. In: *Premier congrès international de spéléologie*. Paris, Tome II, pp 325–333.
- Dublyansky, Y., Moseley, G.E., Lyakhnitsky, Y., Cheng, H., Edwards, L.R., Scholz, D., Koltai, G., Spötl, C., 2018. Late Palaeolithic cave art and permafrost in the Southern Ural. *Sci. Rep.* 8, 12080. <https://doi.org/10.1038/s41598-018-30049-w>
- Fankhauser, A., McDermott, F., Fleitmann, D., 2016. Episodic speleothem deposition tracks the terrestrial impact of millennial-scale last glacial climate variability in SW Ireland. *Quat. Sci. Rev.* 152, 104–117. <https://doi.org/10.1016/j.quascirev.2016.09.019>
- Feuillet, T., 2011. Statistical Analyses of Active Patterned Ground Occurrence in the Taillon Massif (Pyrénées, France/Spain). *Permafr. Periglac. Process.* 22, 228–238. <https://doi.org/10.1002/ppp.726>
- García-Ruiz, J.M., Palacios, D., Andrés, N. de, Valero-Garcés, B.L., López-Moreno, J.I., Sanjuán, Y., 2014. Holocene and 'Little Ice Age' glacial activity in the Marboré Cirque, Monte Perdido Massif, Central Spanish Pyrenees. *The Holocene* 24, 1439–1452. <https://doi.org/10.1177/0959683614544053>
- García-Ruiz, J.M., Palacios, D., Andrés, N., López-Moreno, J.I., 2020. Neoglaciation in the Spanish Pyrenees: a multiproxy challenge. *Mediterr. Geosci. Rev.* 2, 21–36. <https://doi.org/10.1007/s42990-020-00022-9>
- Gázquez, F., Bauska, T.K., Comas-Bru, L., Ghaleb, B., Calaforra, J.-M., Hodell, D.A., 2020. The potential of gypsum speleothems for paleoclimatology: application to the Iberian Roman Humid Period. *Sci. Rep.* 10, 14705. <https://doi.org/10.1038/s41598-020-71679-3>
- Gázquez, F., Calaforra, J.M., Evans, N.P., Hodell, D.A., 2017. Using stable isotopes ( $\delta^{17}\text{O}$ ,  $\delta^{18}\text{O}$  and  $\delta\text{D}$ ) of gypsum hydration water to ascertain the role of water condensation in the formation of subaerial gypsum speleothems. *Chem. Geol.* 452, 34–46. <https://doi.org/10.1016/j.chemgeo.2017.01.021>
- Gellatly, A.F., Grove, J.M., Switsur, V.R., 1992. Mid-Holocene glacial activity in the Pyrenees. *The Holocene* 2, 266–270. <https://doi.org/10.1177/095968369200200309>
- Giesemann, A., Jaeger, H.-J., Norman, A.L., Krouse, H.R., Brand, W.A., 1994. Online Sulfur-Isotope Determination Using an Elemental Analyzer Coupled to a Mass Spectrometer. *Anal. Chem.* 66, 2816–2819. <https://doi.org/10.1021/ac00090a005>
- Gomez Lende, M., Berenguer, F., Serrano, E., 2014. Morphology, ice types and thermal regime in a high mountain ice cave. First studies applying terrestrial laser scanner in the Ppeña

924 Ceastil ice cave (Picos de Europa, Northern Spain). *Geogr. Fis. E Din. Quat.* 37, 141–150.  
925 <https://doi.org/10.4461/GFDQ.2014.37.13>

926 Gómez Lende, M., Serrano, E., Bordehore, L.J., Sandoval, S., 2016. The role of GPR techniques  
927 in determining ice cave properties: Peña Castil ice cave, Picos de Europa. *Earth Surf.*  
928 *Process. Landf.* 41, 2177–2190. <https://doi.org/10.1002/esp.3976>

929 Gómez-Ortiz, A., Oliva, M., Salvador-Franch, F., Palacios, D., Tanarro, L.M., de Sanjosé-Blasco,  
930 J.J., Salvà-Catarineu, M., 2019. Monitoring permafrost and periglacial processes in  
931 Sierra Nevada (Spain) from 2001 to 2016. *Permafr. Periglac. Process.* 30, 278–291.  
932 <https://doi.org/10.1002/ppp.2002>

933 González Trueba, J.J., Moreno, R.M., Martínez de Pisón, E., Serrano, E., 2008. ‘Little Ice Age’  
934 glaciation and current glaciers in the Iberian Peninsula. *The Holocene* 18, 551–568.  
935 <https://doi.org/10.1177/0959683608089209>

936 Gruber, S., Haeberli, W., 2009. Mountain Permafrost, in: Margesin, R. (Ed.), *Permafrost Soils,*  
937 *Soil Biology.* Springer, Berlin, Heidelberg, pp. 33–44. [https://doi.org/10.1007/978-3-](https://doi.org/10.1007/978-3-540-69371-0_3)  
938 [540-69371-0\\_3](https://doi.org/10.1007/978-3-540-69371-0_3)

939 Gubler, S., Fiddes, J., Keller, M., Gruber, S., 2011. Scale-dependent measurement and analysis  
940 of ground surface temperature variability in alpine terrain. *The Cryosphere* 5, 431–443.  
941 <https://doi.org/10.5194/tc-5-431-2011>

942 Haeberli, W., Rellstab, W., Harrison, W.D., 1984. Geothermal Effects of 18 ka BP Ice Conditions  
943 in the Swiss Plateau. *Ann. Glaciol.* 5, 56–60. [https://doi.org/10.3189/1984AoG5-1-56-](https://doi.org/10.3189/1984AoG5-1-56-60)  
944 [60](https://doi.org/10.3189/1984AoG5-1-56-60)

945 Harris, C., Vonder Mühll, D., Isaksen, K., Haeberli, W., Sollid, J.L., King, L., Holmlund, P., Dramis,  
946 F., Guglielmin, M., Palacios, D., 2003. Warming permafrost in European mountains.  
947 *Glob. Planet. Change* 39, 215–225. <https://doi.org/10.1016/j.gloplacha.2003.04.001>

948 Heeb, B., 2014. The Next Generation of the DistoX Cave Surveying Instrument. *CREG J.*, 88, 5–8.

949 Hercman, H., Gąsiorowski, M., Gradziński, M., Kicińska, D., 2010. The First Dating of Cave Ice  
950 from the Tatra Mountains, Poland and its Implication to Palaeoclimate  
951 Reconstructions. *Geochronometria* 36, 31–38. [https://doi.org/10.2478/v10003-010-](https://doi.org/10.2478/v10003-010-0016-2)  
952 [0016-2](https://doi.org/10.2478/v10003-010-0016-2)

953 Hill, C.A., 1987. Geology of Carlsbad Cavern and other caves in the Guadalupe Mountains, New  
954 Mexico and Texas. *Bull 117 N. M. Bur. Mines Miner. Resour.*

955 Hock, R., Rasul, G., Adler, C., Cáceres, B., Gruber, S., Hirabayashi, Y., Jackson, J., Kääb, A., Kang,  
956 S., Kutuzov, S., Milner, A., Molau, U., Morin, S., Orlove, B., Steltzer, H., 2019. High  
957 Mountain Areas. In: *IPCC Special Report on the Ocean and Cryosphere in a Changing*  
958 *Climate.*

959 Kern, Z., Bočić, N., Sipos, G., 2018. Radiocarbon-Dated Vegetal Remains from the Cave Ice  
960 Deposits of Velebit Mountain, Croatia. *Radiocarbon* 60, 1391–1402.  
961 <https://doi.org/10.1017/RDC.2018.108>

962 Kern, Z., Perşoiu, A., 2013. Cave ice – the imminent loss of untapped mid-latitude cryospheric  
963 palaeoenvironmental archives. *Quat. Sci. Rev.* 67, 1–7.  
964 <https://doi.org/10.1016/j.quascirev.2013.01.008>

965 Koltai, G., Spötl, C., Cheng, H., 2020. Cryogenic cave carbonates in the Dolomites (Northern  
966 Italy): insights into Younger Dryas cooling and seasonal precipitation. *Clim. Past*  
967 *Discuss.* 1–25. <https://doi.org/10.5194/cp-2020-107>

968 Korshunov, V.V., Shavrina, E.V., 1998. Gypsum speleothems of freezing origin. *J. Cave Karst*  
969 *Stud.* 60, 146–150.

970 Lechleitner, F.A., Mason, A.J., Breitenbach, S.F.M., Vaks, A., Haghipour, N., Henderson, G.M.,  
971 2020. Permafrost-related hiatuses in stalagmites: Evaluating the potential for  
972 reconstruction of carbon cycle dynamics. *Quat. Geochronol.* 56, 101037.  
973 <https://doi.org/10.1016/j.quageo.2019.101037>

974 Leunda, M., González-Sampériz, P., Gil-Romera, G., Bartolomé, M., Belmonte-Ribas, Á., Gómez-  
975 García, D., Kaltenrieder, P., Rubiales, J.M., Schwörer, C., Tinner, W., Morales-Molino,



976 C., Sancho, C., 2019. Ice cave reveals environmental forcing of long-term Pyrenean tree  
 977 line dynamics. *J. Ecol.* 107, 814–828. <https://doi.org/10.1111/1365-2745.13077>

978 Lewkowicz, A.G., Ednie, M., 2004. Probability mapping of mountain permafrost using the BTS  
 979 method, Wolf Creek, Yukon Territory, Canada. *Permafr. Periglac. Process.* 15, 67–80.  
 980 <https://doi.org/10.1002/ppp.480>

981 Li, T.-Y., Baker, J.L., Wang, T., Zhang, J., Wu, Y., Li, H.-C., Blyakharchuk, T., Yu, T.-L., Shen, C.-C.,  
 982 Cheng, H., Kong, X.-G., Xie, W.-L., Edwards, R.L., 2021. Early Holocene permafrost  
 983 retreat in West Siberia amplified by reorganization of westerly wind systems.  
 984 *Commun. Earth Environ.* 2, 1–11. <https://doi.org/10.1038/s43247-021-00238-z>

985 López-Moreno, J.I., Alonso-González, E., Monserrat, O., Del Río, L.M., Otero, J., Lapazaran, J.,  
 986 Luzi, G., Dematteis, N., Serreta, A., Rico, I., Serrano-Cañadas, E., Bartolomé, M.,  
 987 Moreno, A., Buisan, S., Revuelto, J., 2019. Ground-based remote-sensing techniques  
 988 for diagnosis of the current state and recent evolution of the Monte Perdido Glacier,  
 989 Spanish Pyrenees. *J. Glaciol.* 65, 85–100. <https://doi.org/10.1017/jog.2018.96>

990 López-Moreno, J.I., Revuelto, J., Rico, I., Chueca-Cía, J., Julián, A., Serreta, A., Serrano, E.,  
 991 Vicente-Serrano, S.M., Azorin-Molina, C., Alonso-González, E., García-Ruiz, J.M., 2016.  
 992 Thinning of the Monte Perdido Glacier in the Spanish Pyrenees since 1981. *The*  
 993 *Cryosphere* 10, 681–694. <https://doi.org/10.5194/tc-10-681-2016>

994 Losiak, A., Derkowski, A., Skała, A., Trzciński, J., 2016. Evaporites on ice: how to form gypsum  
 995 on Antarctica and on Martian North polar residual cap? In: 47th Lunar and Planetary  
 996 Science Conference. 1972.pdf.

997 Luetscher, M., Bolius, D., Schwikowski, M., Schotterer, U., Smart, P.L., 2007. Comparison of  
 998 techniques for dating of subsurface ice from Monlesi ice cave, Switzerland. *J. Glaciol.*  
 999 53, 374–384.

1000 Luetscher, M., Borreguero, M., Moseley, G.E., Spötl, C., Edwards, R.L., 2013. Alpine permafrost  
 1001 thawing during the Medieval Warm Period identified from cryogenic cave carbonates.  
 1002 *The Cryosphere* 7, 1073–1081. <https://doi.org/10.5194/tc-7-1073-2013>

1003 Luetscher, M., Jeannin, P.-Y., 2018. Chapter 12 - Ice Caves in Switzerland, in: Perçoiu, A.,  
 1004 Lauritzen, S.-E. (Eds.), *Ice Caves*. Elsevier, pp. 221–235. <https://doi.org/10.1016/B978-0-12-811739-2.00010-3>

1006 Luetscher, M., Lismonde, B., Jeannin, P.-Y., 2008. Heat exchanges in the heterothermic zone of  
 1007 a karst system: Monlesi cave, Swiss Jura Mountains. *J. Geophys. Res. Earth Surf.* 113.  
 1008 <https://doi.org/10.1029/2007JF000892>

1009 Lundberg, J., McFarlane, D.A., 2007. Pleistocene depositional history in a periglacial terrane: A  
 1010 500 k.y. record from Kents Cavern, Devon, United Kingdom. *Geosphere* 3, 199–219.  
 1011 <https://doi.org/10.1130/GES00085.1>

1012 Marshall, P., Brown, M.C., 1974. Ice in Coulthard Cave, Alberta. *Can. J. Earth Sci.*  
 1013 <https://doi.org/10.1139/e74-045>

1014 Mavlyudov, B.R., 2008. Caves Glaciation in the Past. Федеральное государственное  
 1015 бюджетное учреждение науки Институт географии Российской академии наук, pp.  
 1016 499–505.

1017 Moseley, G.E., Edwards, R.L., Lord, N.S., Spötl, C., Cheng, H., 2021. Speleothem record of mild  
 1018 and wet mid-Pleistocene climate in northeast Greenland. *Sci. Adv.* 7, eabe1260.  
 1019 <https://doi.org/10.1126/sciadv.abe1260>

1020 Munroe, J., Kimble, K., Spötl, C., Marks, G.S., McGee, D., Herron, D., 2021. Cryogenic cave  
 1021 carbonate and implications for thawing permafrost at Winter Wonderland Cave, Utah,  
 1022 USA. *Sci. Rep.* 11, 6430. <https://doi.org/10.1038/s41598-021-85658-9>

1023 Munroe, J.S., 2021. First investigation of perennial ice in Winter Wonderland Cave, Uinta  
 1024 Mountains, Utah, USA. *The Cryosphere* 15, 863–881. <https://doi.org/10.5194/tc-15-863-2021>

1026 Navarro-Serrano, F., López-Moreno, J.I., Azorin-Molina, C., Alonso-González, E., Tomás-  
 1027 Burguera, M., Sanmiguel-Valladolid, A., Revuelto, J., Vicente-Serrano, S.M., 2018.

1028 Estimation of near-surface air temperature lapse rates over continental Spain and its  
1029 mountain areas. *Int. J. Climatol.* 38, 3233–3249. <https://doi.org/10.1002/joc.5497>  
1030 Noetzli, J., Gruber, S., 2009. Transient thermal effects in Alpine permafrost. *The Cryosphere* 3,  
1031 85–99. <https://doi.org/10.5194/tc-3-85-2009>  
1032 Orvošová, M., Deininger, M., Milovský, R., 2014. Permafrost occurrence during the Last  
1033 Permafrost Maximum in the Western Carpathian Mountains of Slovakia as inferred  
1034 from cryogenic cave carbonate. *Boreas* 43, 750–758.  
1035 <https://doi.org/10.1111/bor.12042>  
1036 Perşoiu, A., Buzjak, N., Onaca, A., Pennos, C., Sotiriadis, Y., Ionita, M., Zachariadis, S., Styllas,  
1037 M., Kosutnik, J., Hegyi, A., Butorac, V., 2021. Record summer rains in 2019 led to  
1038 massive loss of surface and cave ice in SE Europe. *The Cryosphere* 15, 2383–2399.  
1039 <https://doi.org/10.5194/tc-15-2383-2021>  
1040 Perşoiu, A., Lauritzen, S.-E. (Eds.), 2018. *Ice caves*. Elsevier, Amsterdam, Netherlands.  
1041 Perşoiu, A., Onac, B.P., Wynn, J.G., Blaauw, M., Ionita, M., Hansson, M., 2017. Holocene winter  
1042 climate variability in Central and Eastern Europe. *Sci. Rep.* 7, 1196.  
1043 <https://doi.org/10.1038/s41598-017-01397-w>  
1044 Pons, X., Ninyerola, M., 2008. Mapping a topographic global solar radiation model  
1045 implemented in a GIS and refined with ground data. *Int. J. Climatol.* 28, 1821–1834.  
1046 <https://doi.org/10.1002/joc.1676>  
1047 Racine, T.M.F., Spötl, C., Reimer, P.J., Čarga, J., 2022. RADIOCARBON CONSTRAINTS ON  
1048 PERIODS OF POSITIVE CAVE ICE MASS BALANCE DURING THE LAST MILLENNIUM,  
1049 JULIAN ALPS (NW SLOVENIA). *Radiocarbon* 1–24.  
1050 <https://doi.org/10.1017/RDC.2022.26>  
1051 Reille, M., Andrieu, V., 1995. The late Pleistocene and Holocene in the Lourdes Basin, Western  
1052 Pyrénées, France: new pollen analytical and chronological data. *Veg. Hist.*  
1053 *Archaeobotany* 4, 1–21. <https://doi.org/10.1007/BF00198611>  
1054 Requirand, C., 2014. Hypothèse sur la formation des cristaux de gypse Grotte Glacée Devaux  
1055 (Gavarnie - Hautes Pyrénées). *Bulletin de la Société Ramon.* 11 pp.  
1056 Richter, D.K., Meissner, P., Immenhauser, A., Schulte, U., Dorsten, I., 2010a. Cryogenic and  
1057 non-cryogenic pool calcites indicating permafrost and non-permafrost periods: a case  
1058 study from the Herbstlabyrinth-Advent Cave system (Germany). *The Cryosphere* 4,  
1059 501–509. <https://doi.org/10.5194/tc-4-501-2010>  
1060 Richter, D.K., Meissner, P., Immenhauser, A., Schulte, U., Dorsten, I., 2010b. Cryogenic and  
1061 non-cryogenic pool calcites indicating permafrost and non-permafrost periods: a case  
1062 study from the Herbstlabyrinth-Advent Cave system (Germany). *The Cryosphere* 4,  
1063 501–509. <https://doi.org/10.5194/tc-4-501-2010>  
1064 Rico, I., Magnin, F., López Moreno, J.I., Serrano, E., Alonso-González, E., Revuelto, J., Hughes-  
1065 Allen, L., Gómez-Lende, M., 2021. First evidence of rock wall permafrost in the  
1066 Pyrenees (Vignemale peak, 3,298 m a.s.l., 42°46′16″N/0°08′33″W). *Permafr. Periglac.*  
1067 *Process.* 32, 673–680. <https://doi.org/10.1002/ppp.2130>  
1068 Rodríguez-Salgado, P., Oms, O., Ibáñez-Insa, J., Anadón, P., Gómez de Soler, B., Campeny, G.,  
1069 Agustí, J., 2021. Mineralogical proxies of a Pliocene maar lake recording changes in  
1070 precipitation at the Camp dels Ninots (Pliocene, NE Iberia). *Sediment. Geol.* 418,  
1071 105910. <https://doi.org/10.1016/j.sedgeo.2021.105910>  
1072 Rösch, G., Rösch, J., 1935. Visites à la grotte Devaux. *La Montagne. Revue du Club Alpin*  
1073 *Français*, N° 269, pp.171-178.  
1074 Rösch, J., 1949. Une exploration de la Grotte Devaux à Gavarnie. *Bulletin de la section du Sud-*  
1075 *Ouest de la Club Alpin Français*, N°69. pp. 103-107.  
1076 Sancho, C., Arenas, C., Pardo, G., Peña-Monné, J.L., Rhodes, E.J., Bartolomé, M., García-Ruiz,  
1077 J.M., Martí-Bono, C., 2018a. Glaciolacustrine deposits formed in an ice-dammed  
1078 tributary valley in the south-central Pyrenees: New evidence for late Pleistocene  
1079 climate. *Sediment. Geol.* 366, 47–66. <https://doi.org/10.1016/j.sedgeo.2018.01.008>

1080 Sancho, C., Belmonte, Á., Bartolomé, M., Moreno, A., Leunda, M., López-Martínez, J., 2018b.  
 1081 Middle-to-late Holocene palaeoenvironmental reconstruction from the A294 ice-cave  
 1082 record (Central Pyrenees, northern Spain). *Earth Planet. Sci. Lett.* 484, 135–144.  
 1083 <https://doi.org/10.1016/j.epsl.2017.12.027>  
 1084 Sancho, C., Peña, J.L., Mikkan, R., Osácar, C., Quinif, Y., 2004. Morphological and speleothemic  
 1085 development in Brujas Cave (Southern Andean Range, Argentina):  
 1086 palaeoenvironmental significance. *Geomorphology* 57, 367–384.  
 1087 [https://doi.org/10.1016/S0169-555X\(03\)00166-1](https://doi.org/10.1016/S0169-555X(03)00166-1)  
 1088 Scandroglio, R., Draebing, D., Offer, M., Krautblatter, M., 2021. 4D quantification of alpine  
 1089 permafrost degradation in steep rock walls using a laboratory-calibrated electrical  
 1090 resistivity tomography approach. *Surf. Geophys.* 19, 241–260.  
 1091 <https://doi.org/10.1002/nsg.12149>  
 1092 Seal, R.R., II, 2006. Sulfur Isotope Geochemistry of Sulfide Minerals. *Rev. Mineral. Geochem.*  
 1093 61, 633–677. <https://doi.org/10.2138/rmg.2006.61.12>  
 1094 Serrano, E., Gómez-Lende, M., Belmonte, Á., Sancho, C., Sánchez-Benítez, J., Bartolomé, M.,  
 1095 Leunda, M., Moreno, A., Hivert, B., 2018. Chapter 28 - Ice Caves in Spain, in: Perşoiu,  
 1096 A., Lauritzen, S.-E. (Eds.), *Ice Caves*. Elsevier, pp. 625–655.  
 1097 <https://doi.org/10.1016/B978-0-12-811739-2.00028-0>  
 1098 Serrano, E., López-Moreno, J.I., Gómez-Lende, M., Pisabarro, A., Martín-Moreno, R., Rico, I.,  
 1099 Alonso-González, E., 2020. Frozen ground and periglacial processes relationship in  
 1100 temperate high mountains: a case study at Monte Perdido-Tucarroya area (The  
 1101 Pyrenees, Spain). *J. Mt. Sci.* 17, 1013–1031. [https://doi.org/10.1007/s11629-019-5614-](https://doi.org/10.1007/s11629-019-5614-5)  
 1102 5  
 1103 Serrano, E., Sanjosé-Blasco, J.J. de, Gómez-Lende, M., López-Moreno, J.I., Pisabarro, A.,  
 1104 Martínez-Fernández, A., 2019. Periglacial environments and frozen ground in the  
 1105 central Pyrenean high mountain area: Ground thermal regime and distribution of  
 1106 landforms and processes. *Permafr. Periglac. Process.* 30, 292–309.  
 1107 <https://doi.org/10.1002/ppp.2032>  
 1108 Spötl, C., Cheng, H., 2014. Holocene climate change, permafrost and cryogenic carbonate  
 1109 formation: insights from a recently deglaciated, high-elevation cave in the Austrian  
 1110 Alps. *Clim. Past* 10, 1349–1362. <https://doi.org/10.5194/cp-10-1349-2014>  
 1111 Spötl, C., Koltai, G., Jarosch, A.H., Cheng, H., 2021. Increased autumn and winter precipitation  
 1112 during the Last Glacial Maximum in the European Alps. *Nat. Commun.* 12, 1839.  
 1113 <https://doi.org/10.1038/s41467-021-22090-7>  
 1114 Spötl, C., Reimer, P.J., Luetscher, M., 2014. Long-term mass balance of perennial firn and ice  
 1115 in an Alpine cave (Austria): Constraints from radiocarbon-dated wood fragments. *The*  
 1116 *Holocene* 0959683613515729. <https://doi.org/10.1177/0959683613515729>  
 1117 Stoffel, M., Luetscher, M., Bollschweiler, M., Schlatter, F., 2009. Evidence of NAO control on  
 1118 subsurface ice accumulation in a 1200 yr old cave-ice sequence, St. Livres ice cave,  
 1119 Switzerland. *Quat. Res.* 72, 16–26. <https://doi.org/10.1016/j.yqres.2009.03.002>  
 1120 Supper, R., Ottowitz, D., Jochum, B., Römer, A., Pfeiler, S., Kauer, S., Keuschnig, M., Ita, A.,  
 1121 2014. Geoelectrical monitoring of frozen ground and permafrost in alpine areas: field  
 1122 studies and considerations towards an improved measuring technology. *Surf. Geophys.*  
 1123 12, 93–115. <https://doi.org/10.3997/1873-0604.2013057>  
 1124 Temovski, M., Futó, I., Túri, M., Palcsu, L., 2018. Sulfur and oxygen isotopes in the gypsum  
 1125 deposits of the Provalata sulfuric acid cave (Macedonia). *Geomorphology* 315, 80–90.  
 1126 <https://doi.org/10.1016/j.geomorph.2018.05.010>  
 1127 Vaks, A., Gutareva, O.S., Breitenbach, S.F.M., Avirmed, E., Mason, A.J., Thomas, A.L., Osinzev,  
 1128 A.V., Kononov, A.M., Henderson, G.M., 2013. Speleothems Reveal 500,000-Year  
 1129 History of Siberian Permafrost. *Science* 340, 183–186.  
 1130 <https://doi.org/10.1126/science.1228729>

1131 Vaks, A., Mason, A.J., Breitenbach, S.F.M., Kononov, A.M., Osinzev, A.V., Rosensaft, M.,  
 1132 Borshevsky, A., Gutareva, O.S., Henderson, G.M., 2020. Palaeoclimate evidence of  
 1133 vulnerable permafrost during times of low sea ice. *Nature* 577, 221–225.  
 1134 <https://doi.org/10.1038/s41586-019-1880-1>

1135 Wind, M., Obleitner, F., Racine, T., Spötl, C., 2022. Multi-annual temperature evolution and  
 1136 implications for cave ice development in a sag-type ice cave in the Austrian Alps.  
 1137 *Cryosphere Discuss.* 1–26. <https://doi.org/10.5194/tc-2022-67>

1138 Wollenburg, J.E., Katlein, C., Nehrke, G., Nöthig, E.-M., Matthiessen, J., Wolf- Gladrow, D.A.,  
 1139 Nikolopoulos, A., Gázquez-Sanchez, F., Rossmann, L., Assmy, P., Babin, M., Bruyant, F.,  
 1140 Beaulieu, M., Dybwad, C., Peeken, I., 2018. Ballasting by cryogenic gypsum enhances  
 1141 carbon export in a *Phaeocystis* under-ice bloom. *Sci. Rep.* 8, 7703.  
 1142 <https://doi.org/10.1038/s41598-018-26016-0>

1143 Yonge, C.J., Ford, D., Horne, G., Lauriol, B., Schroeder, J., 2018. Chapter 15 - Ice Caves in  
 1144 Canada, in: Perşoiu, A., Lauritzen, S.-E. (Eds.), *Ice Caves*. Elsevier, pp. 285–334.  
 1145 <https://doi.org/10.1016/B978-0-12-811739-2.00015-2>

1146 Žák, K., Onac, B.P., Kadebskaya, O.I., Filippi, M., Dublyansky, Y., Luetscher, M., 2018. Chapter 6  
 1147 - Cryogenic Mineral Formation in Caves, in: Perşoiu, A., Lauritzen, S.-E. (Eds.), *Ice*  
 1148 *Caves*. Elsevier, pp. 123–162. <https://doi.org/10.1016/B978-0-12-811739-2.00035-8>

1149 Žák, K., Richter, D.K., Filippi, M., Živor, R., Deininger, M., Mangini, A., Scholz, D., 2012. Coarsely  
 1150 crystalline cryogenic cave carbonate &ndash; a new archive to estimate the Last  
 1151 Glacial minimum permafrost depth in Central Europe. *Clim. Past* 8, 1821–1837.  
 1152 <https://doi.org/10.5194/cp-8-1821-2012>

1153 Žák, K., Urban, J., Čílek, V., Hercman, H., 2004. Cryogenic cave calcite from several Central  
 1154 European caves: age, carbon and oxygen isotopes and a genetic model. *Chem. Geol.*  
 1155 206, 119–136. <https://doi.org/10.1016/j.chemgeo.2004.01.012>

1156 Zerkle, A.L., Jones, D.S., Farquhar, J., Macalady, J.L., 2016. Sulfur isotope values in the sulfidic  
 1157 Frasassi cave system, central Italy: A case study of a chemolithotrophic S-based  
 1158 ecosystem. *Geochim. Cosmochim. Acta* 173, 373–386.  
 1159 <https://doi.org/10.1016/j.gca.2015.10.028>

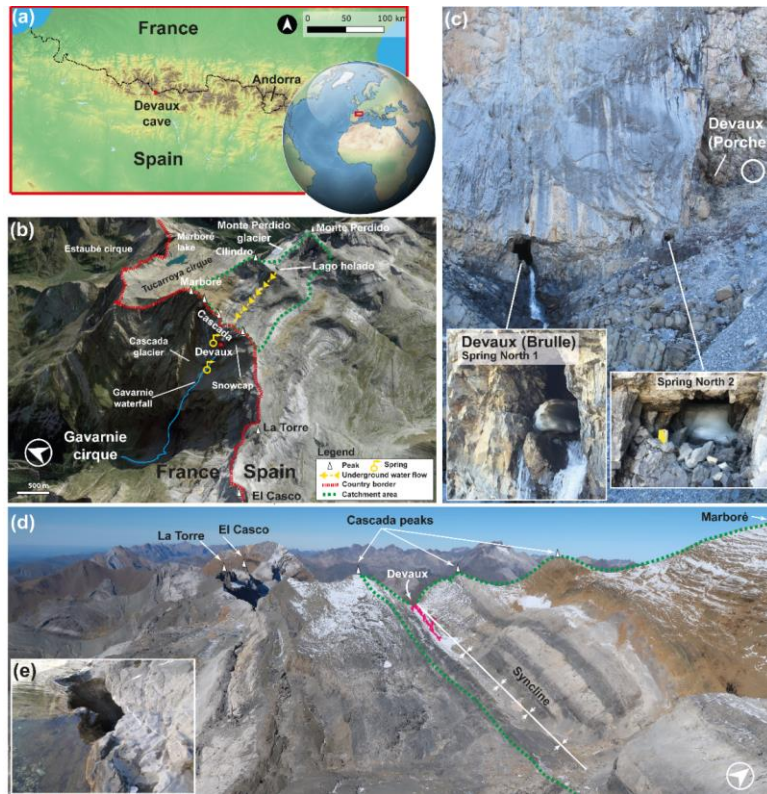


Figure 1. (a) Location of Devaux cave in the Central Pyrenees (ASTER GDEM, NASA v3, 2019). (b) Satellite image and location of Devaux cave, main peaks, lakes, glaciers and cirques in the study area (3D ©Google Earth). The yellow arrows indicate the underground flow path from Lago helado to the Gavarnie waterfall according to the dye-tracing experiment of [du Cailar et al. \(1953\)](#). (c) View towards the entrances of Devaux cave. The lower entrance (~2821 m a.s.l.) corresponds to the Brulle spring (Spring North 1), while the upper one corresponds to the main entrance (Porche (South), ~2836 m a.s.l.). Spring North 2 is located between both entrances. Note person for scale (within the white circle). Remnants of ice partially blocking Brulle and Spring North 2 (July 2021). (d) Landscape view of the catchment area and approximate location of Devaux cave (in dark pink; photo: Paul Cluzon). (e) Ponor located on the southern shore of Lago Helado.

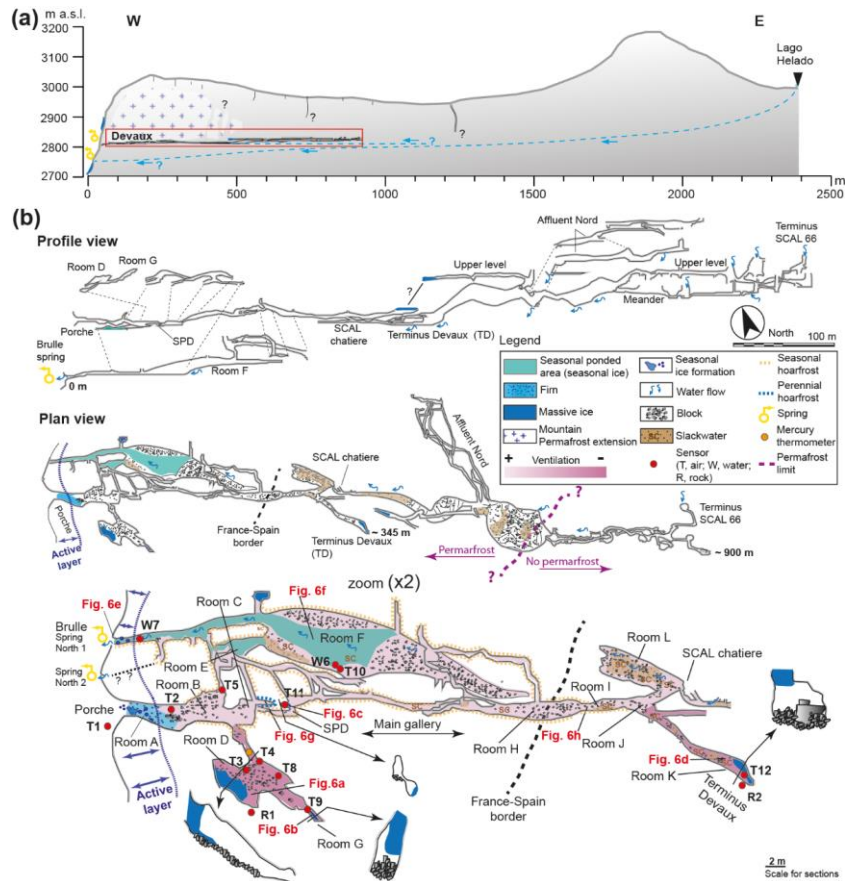


Figure 2. (a) Schematic W-E cross section from Lago Helado to Devaux cave, the assumed extent of mountain permafrost, and ~~and~~ the interpreted underground flow path according to du Cailar et al. (1953). (b) Longitudinal section and plan view of Devaux cave showing the locations of sensors and cave deposits. Labels R, W and T refer to rock, water and air temperature sensors, respectively. The enlarged area corresponds to the first ~345 m of the studied sector. Red labels correspond to the approximate location of the photographs in Fig. 76. Cave survey by Marc Galy, Groupe Spéléologique des Pyrénées (GSPY 86).

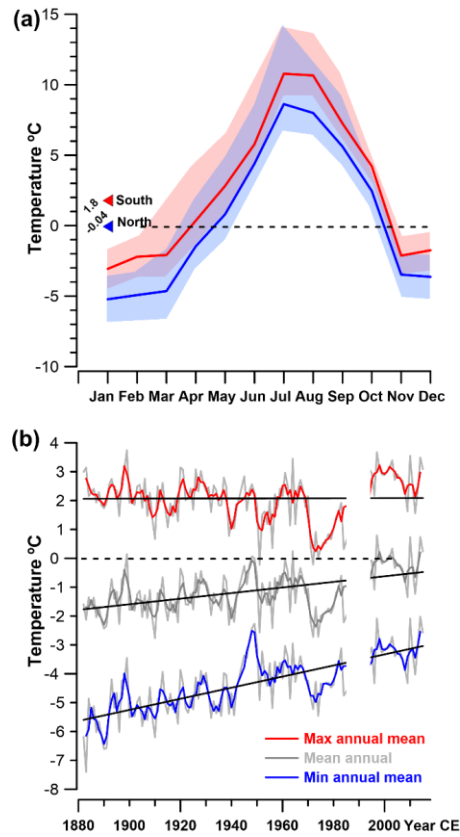


Figure 3. (a) Monthly temperature variation on the northern and southern side of the Monte Perdido massif. Red and blue triangles correspond to the 4-year means. The dashed black line indicates 0°C. Light red and blue shaded envelopes represent the maximum and minimum mean monthly temperatures, respectively. (b) Maximum, mean and minimum annual temperatures recorded at the Pic du Midi de Bigorre station since 1882. Black line indicates the general trend and dashed black line corresponds to 0°C.



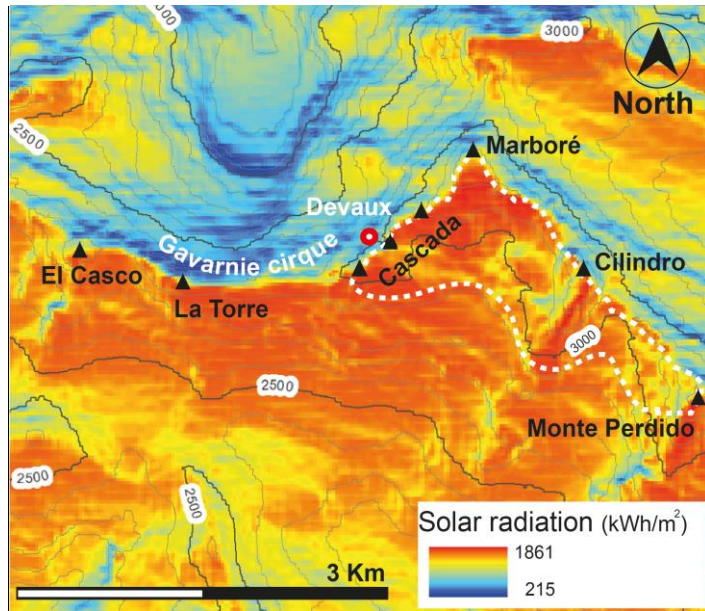


Figure 4. Solar radiation map of the study area. The solar radiation anomaly observed in the Gavarnie cirque is explained by its northerly orientation and the cirque morphology. Black triangles indicate the main peaks above 3000 m. The red-white circle marks Devaux cave, while the dashed white line delineates the approximate catchment.

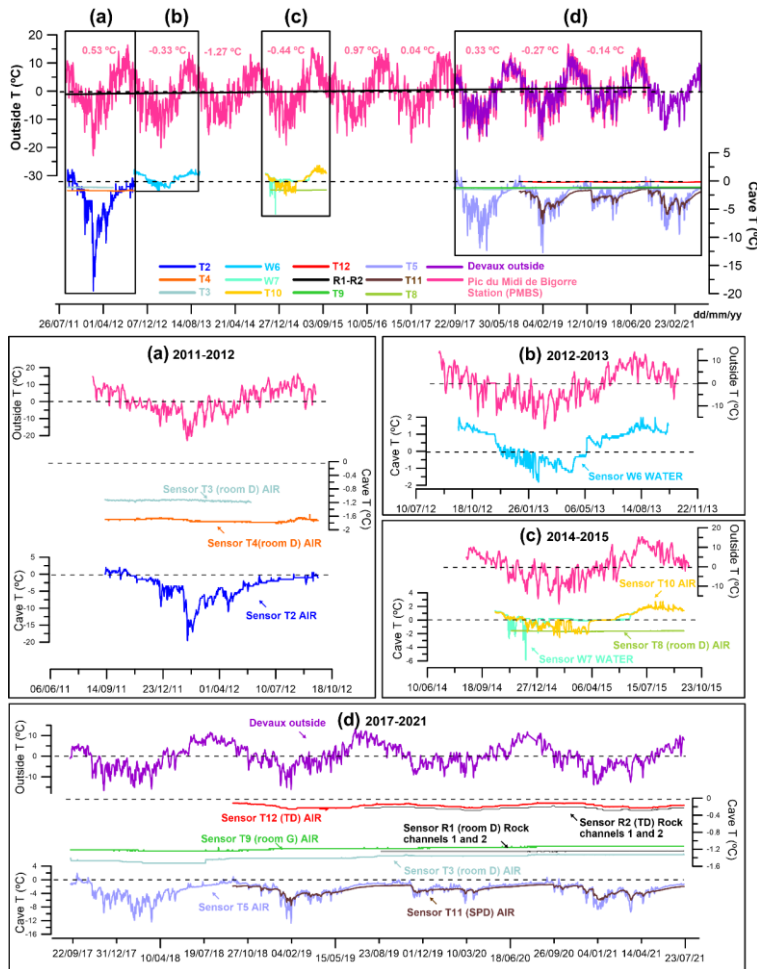


Figure 5. Mean daily air temperature variations at the Pic du Midi de Bigorre station (2860 m a.s.l., red), daily outside air temperature at Devaux cave (2836 m a.s.l., purple) and temperature variations in air, water and rock in the cave for the different time windows since 2011. Dark pink numbers are mean annual air temperatures (MAAT) at the Pic du Midi de Bigorre station (PMBS). Dashed lines indicate 0 °C. Black squares labelled a, b, c, and d correspond to the areas enlarged below. The black continuous line is the external temperature trend during the monitoring period.

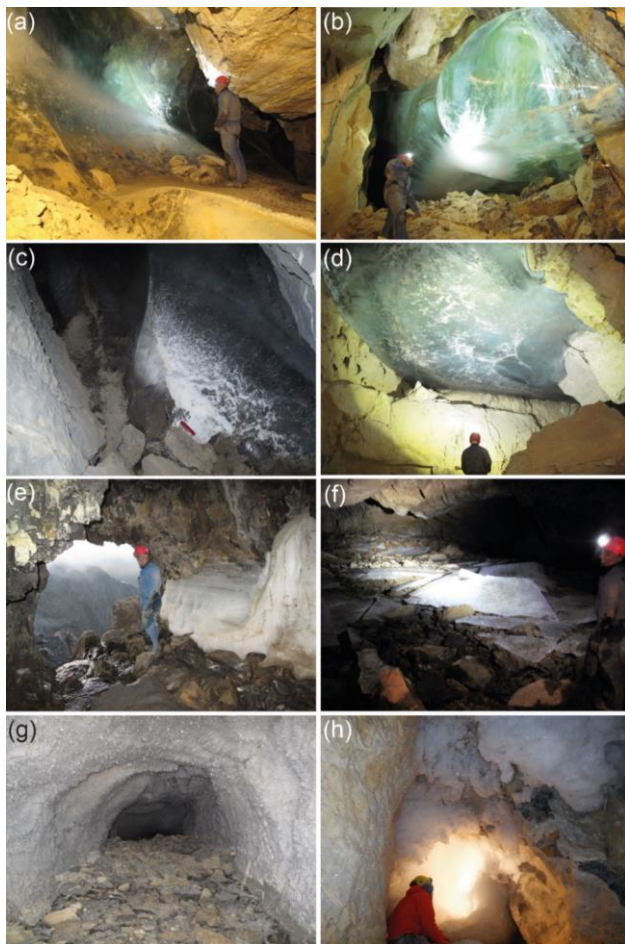


Figure 6. (a) Upper part of the ice body in room D. (b) Ice body hanging from the ceiling and the southwest wall in room G. White colours-spots at near the bottom of the deposit correspond to the concentration of air inclusions as well as cryogenic carbonates and gypsum in the ice. (c) Small ice body in room SPD with CCC-CCG on and within the ice. Red knife (9 cm) for scale. (d) Ice body on the ceiling of room K (Terminus Devaux, TD). (e) Brulle spring and remains of a layered ice body (September 2018). (f) Broken ice sheets in the flooded area in room F (September 2018). (g) Millimetre to centimetre size perennial hoarfrost in a blind gallery below SPD room. (h) Seasonal hoarfrost aggregates (>30 cm long size) covering a cupola close to room J.

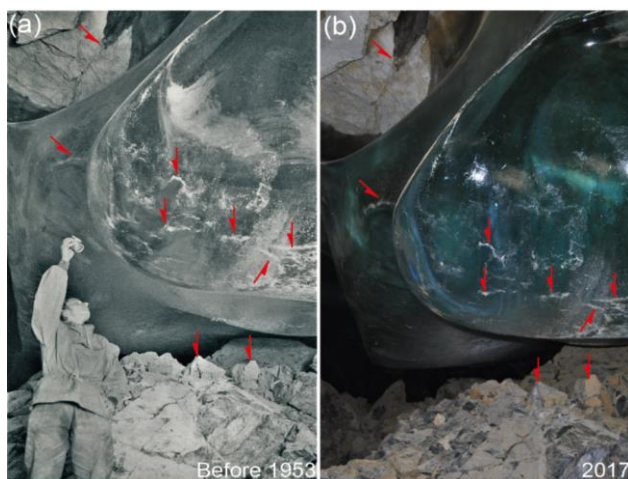


Figure 7. (a) Photo of the ice body located in room G [taken shortly](#) before 1953 ([Casteret, 1953](#)). (b) Photo taken in 2017. In both pictures, white patches on the ice surface correspond to small CCC accumulations released from the ice by sublimation. Red arrows indicate common features in both images.

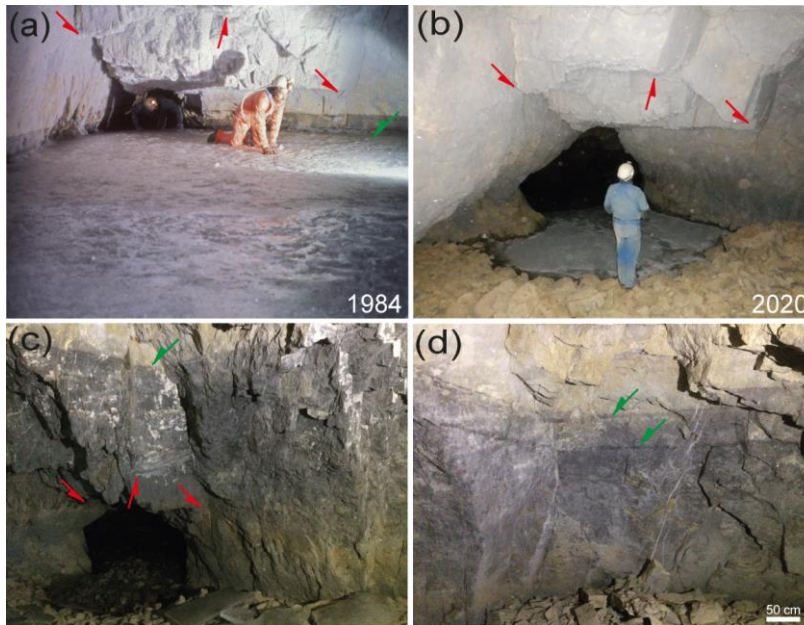


Figure 8. (a) Photo taken close to the river sector that connects the rooms F and E. The estimated ice level is 5 m higher than the Brulle spring. Photo by Jean Luc Bernardin (8<sup>th</sup> August 1984). (b) Similar area in 2020, and maximum extension of the seasonal lake ice formed during winter. (c) Higher ice mark level (c. +9.5 m with respect to the Brulle spring) and remnants of ice sheets from the frozen lake in 2018. (d) Two ice level marks (c. +9.2 m and +8.8 m with respect to the Brulle spring) located between the highest mark and the elevation of the ice in photo (a). In all images red arrows indicate the same rock edges, while green arrows show ice-level marks.



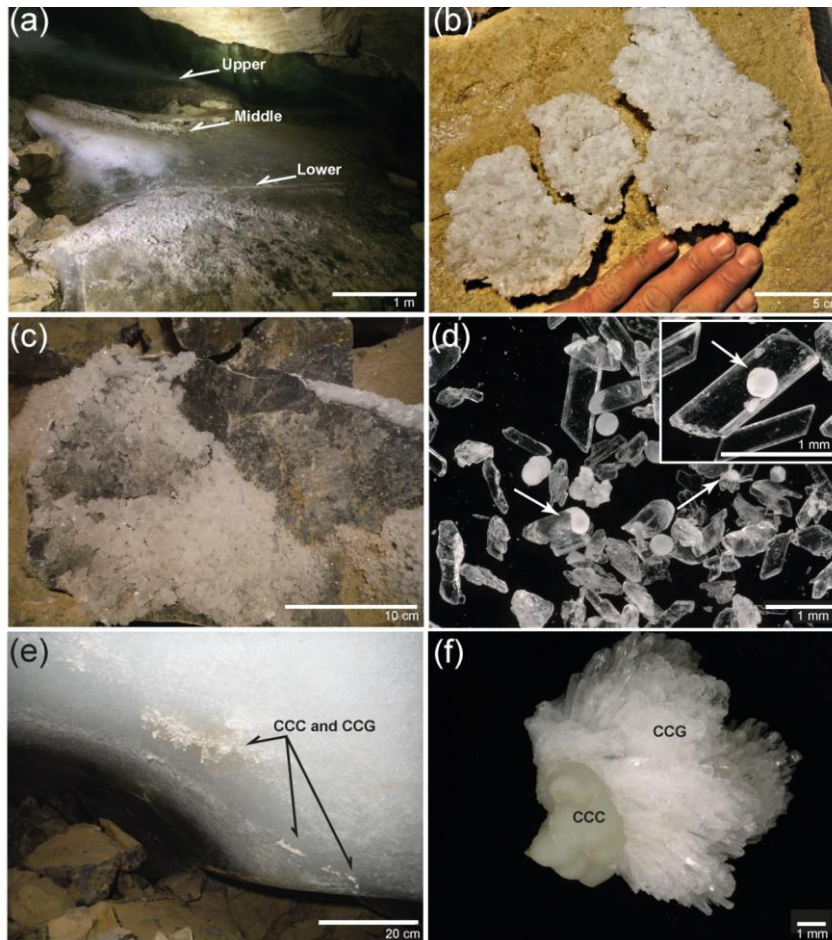


Figure 9. (a) Ice body in room G and three levels marked by cryogenic gypsum partially still in situ in the ice. The white area corresponds to milky ice with a high abundance of air inclusions. Gypsum crystals cover parts of the surface of the ice body due to ice retreat. (b) Large gypsum “raft” deposited on a block in room D. (c) Block in room D with gypsum overgrowths. (d) Microscopic image of euhedral CCG with local-cores of CCC (white arrows), globular CCC, and detail of euhedral gypsum crystal with a core-nucleus of globular CCC. (e) CCC and CCG entrapped within milky ice in room G. (f) Detail of a CCC sample from room G covered by CCG.

Date	Sample	Cations				Anions									
		Na <sup>+</sup>	NH <sub>4</sub> <sup>+</sup>	K <sup>+</sup>	Ca <sup>2+</sup>	Mg <sup>2+</sup>	F <sup>-</sup>	Cl <sup>-</sup>	NO <sub>2</sub> <sup>-</sup>	Br <sup>-</sup>	NO <sub>3</sub> <sup>-</sup>	SO <sub>4</sub> <sup>2-</sup>	HCO <sub>3</sub> <sup>-</sup>	CO <sub>3</sub> <sup>2-</sup>	PO <sub>4</sub> <sup>3-</sup>
15/09/2017	DevauX river 1	1.6	0.0	0.5	36.0	8.5	0.0	0.2	0.0	0.0	1.8	21.6	61.0	11.6	0.0
	DevauX drip 1	0.9	0.1	0.5	50.5	18.2	0.1	0.5	0.0	0.0	6.8	67.4	95.2	0.0	0.0
	DevauX drip 2	1.4	1.2	1.3	53.2	19.5	0.1	1.1	0.1	0.0	7.4	70.1	101.3	0.0	0.0
	DevauX Ice 1 (room D)	2.3	0.0	0.3	24.8	2.7	0.1	1.3	0.0	0.0	0.7	19.0	23.9	1.0	0.0
22/07/2018	DevauX Ice 2 (room D)	2.2	1.3	2.5	27.8	2.0	0.0	2.1	0.0	0.0	1.5	17.0	30.7	0.0	0.0
	DevauX river 1	0.6	0.0	0.4	32.4	4.4	0.0	0.2	0.0	0.0	0.9	5.1	53.7	4.0	0.1
	DevauX river 2	0.6	0.0	0.4	32.2	4.4	0.0	0.2	0.0	0.0	0.9	5.1	56.1	2.6	0.0
	DevauX drip 1	1.4	0.0	3.2	61.0	20.8	0.2	2.2	0.0	0.0	14.1	76.0	84.2	5.6	0.0
22/09/2018	DevauX drip 2	2.3	0.1	1.7	60.8	21.0	0.2	2.2	0.0	0.0	14.1	76.9	91.5	4.4	0.0
	DevauX river 1*	1.3	0.0	0.4	40.5	7.9	0.0	0.3	0.0	0.0	2.0	17.0	65.9	0.0	0.0
	DevauX drip 1*	1.6	0.0	1.2	70.6	27.2	0.2	1.1	0.0	0.0	19.8	116.5	90.3	0.0	0.0
	DevauX ice (seasonal)*	0.4	0.0	0.5	28.2	1.1	0.1	0.5	0.0	0.0	0.5	2.8	36.6	0.0	0.0
28/07/2020	DevauX river 1*	0.6	0.0	0.3	31.5	4.1	0.0	0.2	0.0	0.0	0.8	5.9	58.6	0.0	0.0
	DevauX drip 1*	1.1	0.2	1.1	42.3	12.5	0.1	0.5	0.0	0.0	2.9	38.4	101.3	0.0	0.0
	DevauX drip 2*	1.1	0.1	1.0	43.6	13.5	0.1	0.4	0.0	0.0	2.7	38.2	89.1	0.0	0.0
	DevauX drip 3*	1.6	0.7	1.5	47.9	13.1	0.1	1.1	0.0	0.0	2.2	36.7	107.4	0.0	0.0
26/07/2021	DevauX drip 1	2.9	0.0	1.1	83	35.9	0.3	5.9	0.6	0.1	40.2	269.3	104.9	0.0	0.0
	DevauX drip 2	3.3	0.4	2.0	73.2	29.3	0.2	6.0	0.1	0.0	28.6	212	112.2	0.0	0.0
	DevauX river 1	0.4	0.0	0.1	25.7	4.3	0.1	2.6	0.1	0.0	3.2	16.3	68.3	0.0	0.0
	DevauX river 1	0.7	0.0	0.2	28.6	4.9	0.1	2.6	0.0	0.0	1.5	20.4	74.4	0.0	0.0
13/08/2021	DevauX drip 1	7.5	2.2	5.1	49.5	15.2	0.2	10.3	0.3	0.0	6.9	77.3	130.5	0.0	0.0
	DevauX drip 2	5.1	1.3	2.8	49.3	15.6	0.2	6.5	0.1	0.0	6.5	80.5	129.3	0.0	0.0

Table 1. Chemical composition of water and ice samples from DevauX cave (in mg/l). \* Samples where TDS (total dissolved solids) was calculated.

Location	Sample and description	$\delta^{34}\text{S}$ (‰) VCDT
Room D	Gypsum crystal (part of large raft)	-15.8
Room D	Gypsum crystal (part of large raft)	-15.5
Room D; lower gypsum level	Gypsum crystal (individual)	-15.6
Room D; middle gypsum level	Gypsum crystal (individual)	-15.0
Room D; middle gypsum level	Gypsum crystal (individual)	-15.6
Room D; upper gypsum level	Tiny gypsum crystals (aliquot)	-15.3
Room D	Gypsum crystal (individual)	-15.1
Room G	Gypsum crystal (individual)	-12.3
Room G	Gypsum overgrowth (individual)	-12.1
Room G	Gypsum overgrowth (individual)	-11.9
Room G	Gypsum overgrowth (individual)	-12.1
Room G	Gypsum overgrowth (individual)	-12.0
Limestone above cave	Pyrite crystal (individual)	-12.7
Entrance "Porche"	Drip water (1 liter)	-14.4
Brulle spring	River water 1 (1 liter)	-28.5
Brulle spring	River water 2 (1 liter)	-27.3

Table 2. Sulfur isotope values of gypsum, water and pyrite from Devaux.